UNIVERSITY SAAD DAHLEB BLIDA1

Institute of Aeronautics and Space Studies

MASTER'S THESIS

Specialty: Aeronautics

Option: Propulsion

Numerical modeling of turbulent flow around a SAVONIUS wind turbine

Submitted by

Mihoub Ahmed and Bendjerrat Nabil

A. Bekhti	MRB,	Supervisor
L. Sebaa	MAA, U. Blida 1	Co- Supervisor

Blida, June 2021

ABSTRACT

This thesis presents a numerical modeling of the incompressible and turbulent airflow around a two-bladed Savonius vertical axis wind turbine. The interest of this study is the characterization of the flow downstream of the rotating wind turbine by numerically modeling the generated wake and the power coefficient. The simulation is based on the resolution of Navier Stokes equations in unsteady regime (RANS method) of a flow around a Savonius wind turbine in 2D using the turbulence model komega -SST. The calculations are performed using a computational fluid dynamics (CFD) code (openFoam) based on the finite volume method , the results are presented by the variation of the coefficients of the aerodynamic forces as a function of time. In the second part the simulation is performed for a flow around a two-bladed savonius wind turbine in rotation, the wake is presented by the distribution of speed and vorticity for different angles with respect to several specific velocities.

Key words   : CFD, Vertical axis wind turbine, turbulence, power.

RESUME

Cette thèse présente une modélisation numérique de l'écoulement incompressible et turbulent de l'air autour d'une éolienne à axe vertical Savonius à deux pales. autour d'une éolienne Savonius à axe vertical à deux pales. L'intérêt de cette étude est la caractérisation de l'écoulement en aval de l'éolienne en rotation par la modélisation numérique du sillage généré et du coefficient de puissance. La simulation est basée sur la résolution des équations de Navier Stokes en régime instationnaire (méthode RANS) d'un écoulement autour d'une éolienne Savonius en 2D en utilisant le modèle de turbulence komega -SST. Les calculs sont effectués à l'aide d'un code de dynamique des fluides numérique (CFD) (openFoam) basé sur la méthode des volumes finis, les résultats sont présentés par la variation des coefficients des forces aérodynamiques en fonction du temps. Dans la deuxième partie, la simulation est effectuée pour un écoulement autour d'une éolienne Savonius à deux pales en rotation, le sillage est présenté par la distribution de la vitesse et de la vorticité pour différents angles par rapport à plusieurs vitesses spécifiques.

Mots clés : CFD, éolienne Savonius , axe vertical, turbulent, coefficient de puissance.

الملخص

هذه الأطروحة تعرض نموذجا رقميا لتدفق الهواء المضطرب وغير المعقول حول توربينة الرياح ذات محورين عموديين ويتمثل اهتمام هذه الدراسة في توصيف تدفق التوربين الريحية الدوار إلى أسفل من خلال نمذجة عددية للعواقب المولدة ومعامل الطاقة. وتستند المحاكاة إلى حل معادلات نافيي ستوكس في نظام غير ثابت (طريقة RANS) للتدفق حول اضطراب رياح سافونيوس في2 D باستخدام نموذج الاضطراب komega-SST. ويتم إجراء الحسابات باستخدام رمز ديناميكية السوائل الحسابية استناداً إلى طريقة الحجم المحدود، وتعرض النتائج باختلاف معاملات القوى الأيرودينامية بوصفها وظيفة من وظائف الزمن. في الجزء الثاني يتم إجراء المحاكاة للتدفق حول توربين رياح سافونيوس ذو شفتين في الدوران، يتم عرض التوابع عن طريق توزيع السرعة والمرونة لزوايا مختلفة فيما يتعلق بعدة سرعات محددة.

ACKNOWLEDGEMENTS

TABLE OF CONTENTS

LIST OF FIGURES

LIST OF TABLES

LIST OF SYMBOLS AND ABBREVIATIONS

A: projected area of the rotor m^2.

c_μ : Empirical constant ($= 0.09$).

$C_{1\epsilon}$: Uniform deformation or shear.

$C_{2\epsilon}$: Isotropic turbulent growth.

C_D: Drag coefficient.

C_f : friction coefficient.

C_L: Coefficient of lift.

C_m: Coefficient of moment.

C_p:power coefficient .

E_c:Kinetic energy (J).

F_D: drag (N).

F_L: lift (N).

k: turbulent kinetic energy.

M :Moment $(N.m)$.

m: the weight of the air in (kg).

P: mechanical power (W).

p: Pressure (N/m^2).

P_{wind}:power of the wind incidence (W).

Q :mechanical torque $(N.m)$.

R :radius of the rotor in meters (m).

R_e: Reynolds number.

R_s:overlap relation .

S:the section of air upwind of the rotor m^2.

t: Time (s).

U_∞: Upstream flow velocity (m/s).

U_{fric}: friction speed.

U_T : speed of friction.

V: wind velocity (m/s).

V_0 : occupied air volume (m^3).

x,y: Spatial coordinates (m).

Y :absolute distance from the wall.

y^+: dimensionless distance.

Greek Symbols:

ϵ: Turbulence dissipation rate.

κ: VonKarmen constant .

λ: Tip Speed Ratio.

μ : dynamic viscosity $(kg/m.s)$.

μ_t: turbulent viscosity.

ν: Kinematic viscosity (m^2/s).

ω :rotation speed of rotor (rad/s).

ω: specific turbulent dissipation rate.

ρ: Density (kg/m^3).

σ_k: Comparison with jet-wake experiment.

σ_ϵ: Comparison with jet-wake experiment.

τ_{ij} : Kronecker delta.

τ_W: shear stress .

τ_{wall} : wall friction rate .

τ: Shear stress (N/m^2).

Abbreviations:

CFD: computational fluid dynamics.

DES: Detached Eddy Simulation.

EWT: Environmental Wind Tunnel.

GAMBIT: Geometry And Mesh Building Intelligent Toolkit.

HAWT: horizontal axis wind turbine.

LES: Large Eddy Simulation.

PIMPLE:Pseudo-Implicit Method for Pressure Linked Equations.

RANS: Reynolds averaged Navier Stokes.

Re: Reynolds number.

SIMPLE:Semi-Implicit Method for Pressure Linked Equations.

SST: shear stress transport.

TSR: Tip Speed Ratio.

VAWT: vertical axis wind turbine.

INTRODUCTION

The wind is a free, clean, and inexhaustible energy source. It has served mankind well for many centuries by propelling ships and driving wind turbines to grind grain and pump water. The cost of electricity generated from wind turbines is now comparable to the cost of electricity produced by fossil-fuel-generators. It seems likely that wind power will become a substantial source of electrical power around the world [1].

Wind energy has become the focus of renewable energy research worldwide. And many countries are using wind energy as the basis for their long-term environmental plans, the use of wind energy depends mainly on wind turbines.

Currently, most researchers use numerical simulation methods to analyze the aerodynamic performance of vertical axis wind turbines. The characteristics of VAWT have been demonstrated and compared with those of HAWT, this comparative performance study shows that VAWTs are very simple and cost-effective design, both in terms of manufacturing and maintenance [2].

This work consisted in the numerical modeling of the turbulent flow around a vertical axis wind turbine VAWT of the type SAVONIUS, the main objective is to characterize the flow downstream of the wind turbine in rotation, as well as the study of vorticity field as a function of the characteristic speed.

This thesis consists of five chapters:

The first chapter presents an overview of wind energy, different types of wind turbine and their constitution and operation, also It shows the production of wind energy worldwide and their advantages and disadvantages.

The second chapter consists of a bibliographical review (state of the art) on vertical axis wind turbine of SAVONIUS type .

The third chapter focus on aerodynamics of wind turbines and their performance such as power production, loads and aerodynamic coefficients, also discuss the betz's limit and functional principal of Savonius rotor.

The fourth chapter consists of mathematical and numerical modeling and detailed description of the Navier stocks equations ,In addition the different turbulence models, and the simulation of turbulent flow around Savonius rotor.

The fifth chapter presents and discuss the results of our simulation around a Savonius wind turbine using K omega SST model .
At the end, we have closed our thesis with a conclusion that includes the results obtained

Chapter 1

An overview of wind energy

1.1   Introduction

Energy is one of the main commodities of modern civilization. The amount of energy consumed has become the indicator of the standard of living and the degree of industrialization. Currently, almost ninety percent of the world's energy comes from burning fossil fuels, i.e. coal, oil, natural gas, etc.People use fossil fuels to meet almost all their energy needs, such as powering vehicles, generating electricity for light and heat, and running factories. On the other hand, the earth's fossil fuel energy resources are finite and oil production will exceed its peak in the next few decades. Population growth will make the need for energy more important and the price of fossil fuels higher. At the same time, there is a problem with climate change due to carbon dioxide and sulphur dioxide emissions from burning fossil fuels. Using renewable energy as a cost-effective and reliable low-carbon energy source is becoming an important energy policy objective worldwide. Renewable energy is climate-friendly energy because of the absence of environmentally damaging emissions. The International Energy Agency has indicated that only a very small proportion of energy comes from nuclear and hydroelectric power, and a much smaller proportion from renewable energy sources such as solar, wind, biomass, geothermal and tidal [3]. Wind is an environmentally friendly source of energy that has enormous potential to meet people's energy needs and also to mitigate climate change due to the greenhouse gases emitted by burning fossil fuels. It has been estimated that about 10 million MW of energy is available in the earth's wind. The International Energy Agency (IEA) has shown the cumulative global wind energy capacity worldwide in Figure.(1.1) based on the projection in the World Energy Report 2004 [4].

Wind turbines are used to transform wind energy into mechanical energy (like windmills) and produce electricity. Turbines are classified into two categories, horizontal axis wind tur-
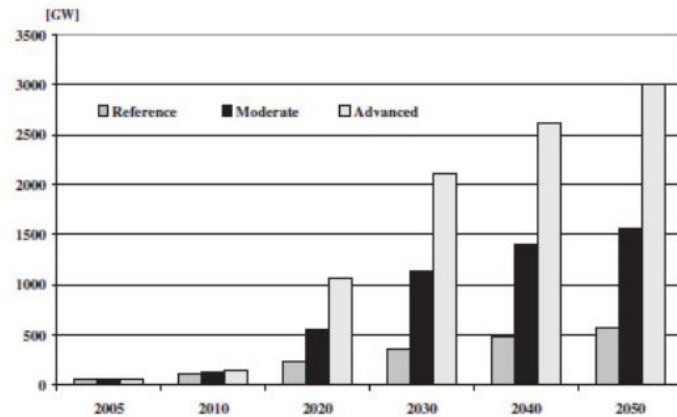
Figure 1.1: Cumulative global wind energy capacity

bines (HAWT) and vertical axis wind turbines (VAWT). If. HAWT has a horizontal rotation axis, then VAWT has a vertical rotation axis. VAWT has a simpler structure and installation than HAWT. The generator of VAWT is placed at the bottom of the central shaft on the ground and the tower does not need to support it. The turbines are useful at different wind speeds and directions [5]. On the other hand, VAWTs have low pressure coefficients, hence significant research on VAWT rotors must improve their performance. VAWT rotors are of different types, such as the Savonius rotor, and (egg beater) Darrieus, or H-Darrieus rotor as shown in Figure. (1.2) [6].
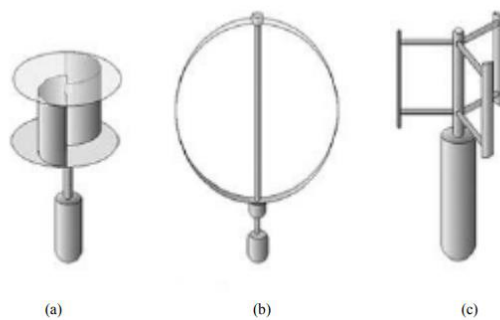
Figure 1.2: Turbines VAWT :(a) rotor Savonius ;(b)rotor Darrieus ;(c) H-Darrieus rotor

17

1.2 History of wind turbines

The first windmill made in the United States was designed by Daniel Halladay, who began inventing windmills in 1854 in his Connecticut machine shop. The windmill was enormously successful as a means of pumping water on the farms and ranches of the expanding western frontier, so much so that Halladay moved his operation to Illinois [7]. The first wind turbine to produce electricity was invented in 1888 in Cleveland, Ohio, by Charles F. Brush. The turbine had a diameter of 17 metres, 144 cedar wood rotor blades and produced about 12 kilowatts (kW) of electricity [8]. Today, the wind industry is booming, driven by rising energy costs and improving technologies. Nearly 12,000 MW in the U.S. and 75,000 MW worldwide have been installed as of early 2007, with a projected growth of 26 % by the end of the year. This potential growth means that wind power could become the second fastest growing energy industry, just behind natural gas [9].

1.3 Global wind energy production

The figure 1.3 [10] illustrates the evolution of global wind power generation capacity in growth from 2000 to 2015 . These statistics show this exponential increase in energy production began with Increase in production from 17.4 GW in 2000 to 432,419 GW in 2015 About 25 times, this shows that the demand for this type of energy is high.
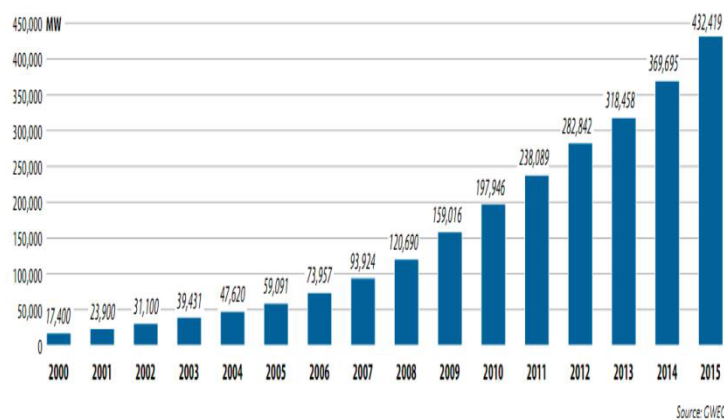
Figure 1.3: The evolution of global wind capacity

1.4 Constitution and operation of a wind turbine

A typical wind turbine is composed of several elements which are presented in the figure 1.4: a mast(tower), a rotor, the nacelle and the blades [11].
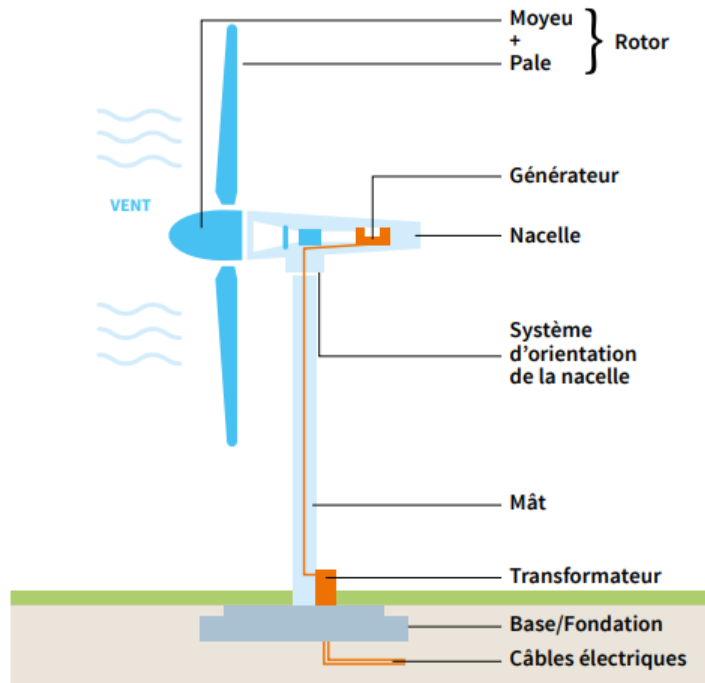
Figure 1.4: Composition of a wind turbine

- the tower : it allows the rotor to move to a sufficient height to allow it to continue moving (required for the horizontal axis wind turbine), the mast has electrical and electronic components (modulators, control multipliers, generators, etc.).

- the rotor: generally composed of three blades and the nose of the wind turbine, it is driven by the wind energy and can be coupled directly or indirectly to a pump (case of pumping wind turbines) or more generally to an electric generator. It is linked to the nacelle by the hub.

- Blades: They are the most important element of the rotor, and they are the converters of the kinetic energy of the wind into mechanical energy (the structure of the blades is related to the aerodynamics and the structure in several points).

- The nacelle: is installed on top of the mast and contains mechanical and pneumatic components and some electrical and electronic components essential to the operation of the machine. The electricity generated in the nacelle is transported to the ground by electrical cables which are located inside the mast of the wind turbine.

The different components of a nacelle (figure 1.5) [12] :

- The speed multiplier is used to increase the speed of rotation between the primary shaft and the secondary shaft that drives the electric generator.

- The secondary shaft usually has a mechanical brake to stop the rotor during maintenance and prevent the machine from running away.

- The generator: this is what converts mechanical energy into electrical energy.

- An electronic controller is in charge of monitoring the operation of the wind turbine. It is in fact a computer capable of managing the start-up of the machine, when the wind speed is sufficient (about 5 m/s) to control the pitch of the blades and brake the direction of the machine, the direction of the "rotor plus nacelle" component facing the wind in order to maximise energy recovery. To perform these different tasks, the controller uses the data provided by the anemometer (wind speed) and wind vane (wind direction), usually located at the back of the nacelle.
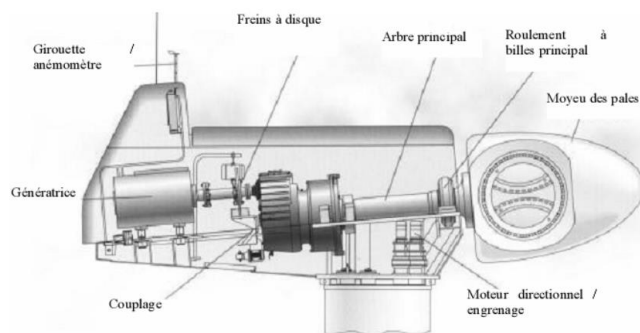
Figure 1.5: Constitution of a nacelle

1.5   Size of wind turbines

Faced with the increase in global electricity consumption, manufacturers tend to produce wind turbines of very strong power therefore of bigger size (figure 1.6) [13] ,since the power captured by the turbine is a function of the square of the rotor radius. According to their nominal power, wind turbines are divided into three categories [14]:

• low power wind turbines: less than 50kW. • Medium power wind turbines: from 50kW to 800kW. • High power wind turbines: greater than 1MW.
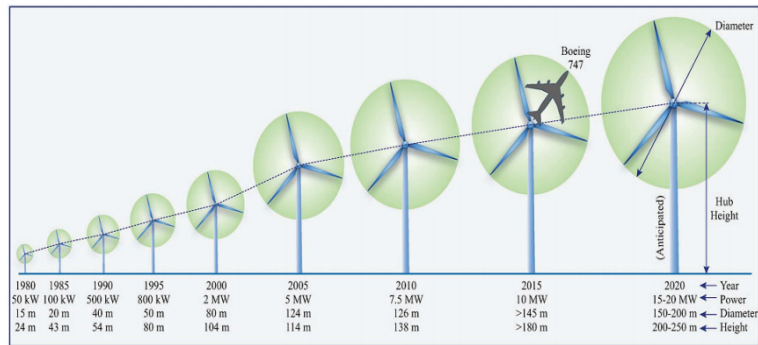
Figure 1.6: Evolution of the size of the wind turbines

1.6 The different types of wind turbines
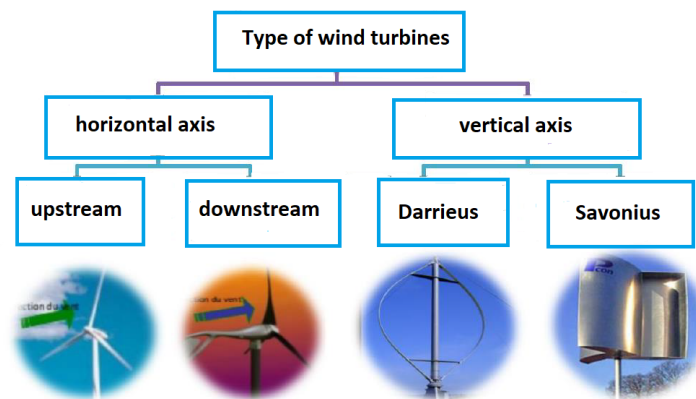
Figure 1.7: Diagram of wind turbine types

The shape of the wind turbine depends primarily on the axis of rotation of the rotor, the part of the wind turbine consisting of the blades, which rotates in the presence of wind. In the technology of wind energy conversion devices, there are two main categories of wind turbines: vertical axis wind turbines and horizontal axis wind turbines. (figure1.7 [15]) .Horizontal axis wind turbines are the most common in the high power wind turbine. The vertical axis wind turbine is more recent, but this type of turbine is experiencing an accelerated development, mainly used small and medium power in urban applications or Domesticated.

1.6.1 Horizontal axis wind turbines

The horizontal axis wind turbines are the most common. They are made of blades whose number can be very variable. For electricity production, we find models with 3 blades and for pumping models with a few dozen blades figure1.8 [16]
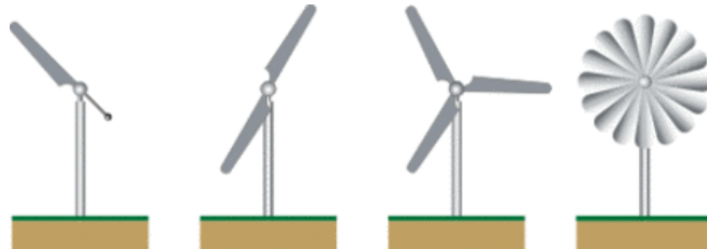
Figure 1.8: wind turbine horizontal axis with different number of blades

1.6.2 Vertical axis wind turbines

There are two main types of vertical axis wind turbines: the Savonius type and the Darrieus type. Their performance is not as good as that of horizontal axis wind turbines. But they have other important advantages: they are less sensitive to to strong winds, start with a lower wind and do not need to be oriented [16]

Darrieus wind turbines

Darrieus vertical axis wind turbines seem to be more suitable than "classical" wind turbines in different areas such as building integration, extreme areas (observatories, mountain refuge...) Although less efficient than three-bladed wind turbines, this type of wind turbine can exceed the limits due to the size of the blades and their speed of rotation, the total size is smaller, and in some cases, when the motor is located at its base, this type of wind turbine can be less expensive. The Darrieus wind turbine can work with wind up to 220 km/h and in any direction, the main drawback of this type of wind turbine is its difficult start, because the weight of the rotor on its base generates friction. Different wind turbines of Darrieus type is illustrated by the figure 1.9
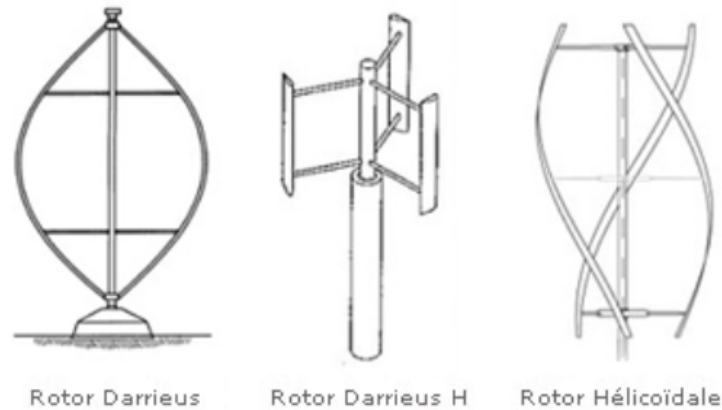
Figure 1.9: Different models of Darrieus vertical axis wind turbines

Savonius wind turbines

The Savonius-type wind turbine, also called S-rotor, was originally invented and patented by the Finnish engineer Sigurd J. Savonius in 1931. The turbine consisted of two half-cylinders, and then the two surfaces of the half-cylinders were moved laterally along the cutting plane as the letter S (see Figure 1.10 [17]). The two semicircular surfaces, called blades or buckets, are mounted on a vertical axis perpendicular to the wind direction, the space between the blades or overlapping it. The Savonius turbine works like a cup anemometer or a drag device. The ratio of the blade tip speed to the wind speed is less than unity because the return blades on the downwind side can never go faster than the wind. Savonius studied the performance of thirty different designs of S-rotors in wind tunnels and in the open air. He reported a maximum power coefficient (Cp) of 0.31 from wind tunnel experiments, while he reported a maximum Cp of 0.37 from open air tests. During the last half century, many researchers have experimented studied the performance of different designs of Savonius wind turbines and obtained Cp numbers in the range of 0.15 to 0.35 [18].

The first of its advantages, and the one that led to its development, is its small size, which can be explained simply by its vertical axis operation. Moreover, the wind turbine is not very noisy if not at all. This is a necessary property if we want to integrate it in urban areas The wind turbine is aesthetic which allows it to be easily integrated into buildings, in collaboration with architects, without distorting the facades. In addition, it starts at low wind speeds of about 2m/s and then has a high torque. It is for this reason that it is sometimes associated with Darrieus wind turbines. It facilitates their drive.
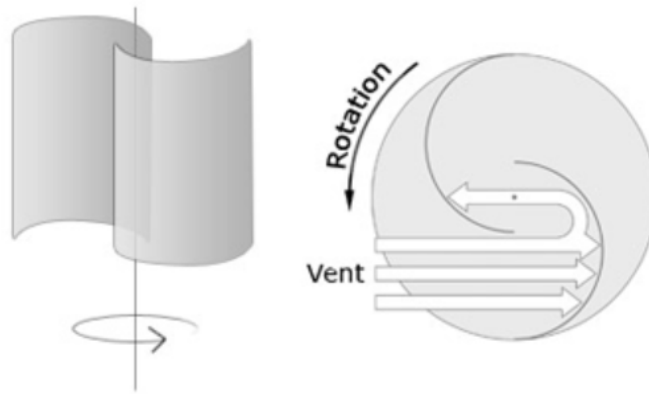
Figure 1.10: Savonius wind turbines

1.7 Different stages of energy conversion

Wind turbines convert wind energy into electrical energy. This conversion takes place in two phases:

-1st phase: at the level of the turbine (rotor) receives part of the kinetic energy of the wind to convert it into mechanical energy [19].

-2nd phase: At the level of the generator, which receives mechanical energy and converts it into electrical energy then transmitted to the electrical network. There must therefore be regular conversion and transmission of energy, the only possibility of storage being inertial at the cost of an acceleration of the turbine [20]. The figure 1.11 [21] illustrates this operation in general :
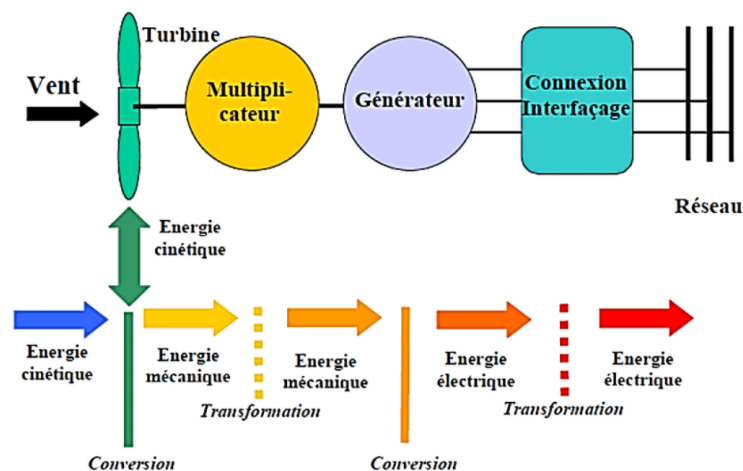
Figure 1.11: Different energy conversion processes

1.8   Noise impact of wind turbines

Noise produced by wind turbines is mainly of two types: mechanical and aerodynamic. Mechanical noise is generated from various machine components within the turbine and is tonal in nature. Aerodynamic noise is generated by the airflow over the blades interacting with the blade surface in various ways, resulting in different sources of aerodynamic noise [22]. A wind turbine produces 55 dB of noise at the base of its tower (figure1.12 [23]), which corresponds to the sound environment of an office. This noise level is generally considered acceptable.
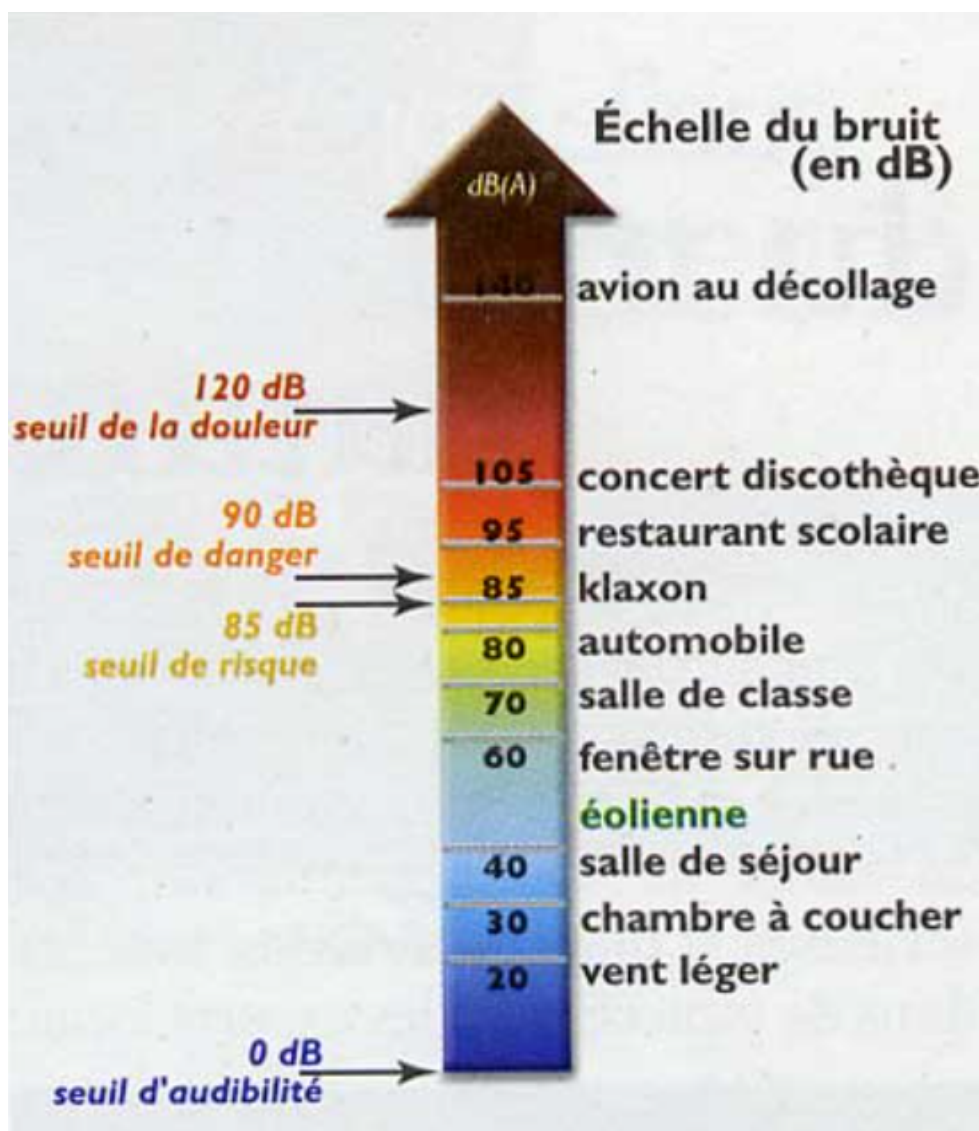
Figure 1.12: noise scale in DB

1.9   Wind energy in Algeria

The Center for the Development of Renewable Energies (CDER), publishes, on the occasion of the winter solstice, a new map of the national wind field. Being engaged in a new phase of exploitation of renewable energies, Algeria plans to reach by 2030 nearly 40% of the national electricity production from renewable sources. Although the choice of solar energy is predominant, wind energy represents the second axis of production of this program. Before studying the possibility of implanting a wind farm in a given region, it is necessary to make studies of the wind deposit for a precise knowledge of the wind meteorology. For this reason, several researchers of the EPST CDER have focused their research in the development of wind maps of Algeria [24] here is a figure1.13.
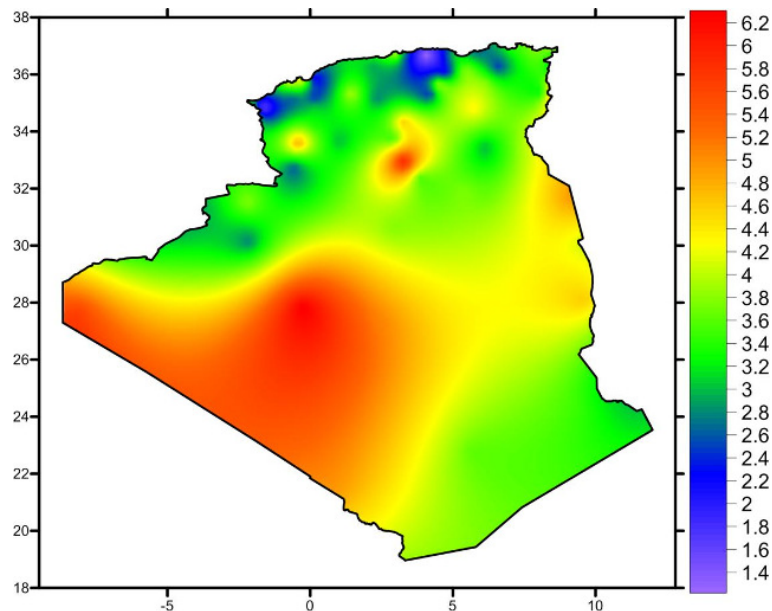
Figure 1.13: Map of wind energy in Algeria

1.10   The advantages and disadvantages of wind energy

1.10.1   The Advantages

- Wind energy is clean and renewable : unlike coal, natural gas or oil, generating electricity from wind does not result in greenhouse gas emissions. While there are some environmental considerations in building large wind farms, once in operation, the turbines themselves

do not need to burn fossil fuels to operate.

- Wind energy has low operating costs: In terms of initial costs, wind farms or individual turbines can be expensive to install. However, once in operation, operating costs are relatively low; their fuel (wind) is free and the turbines do not require much maintenance over their lifetime.

- Wind energy is space efficient: Wind farms may take up a lot of land, but the turbines and equipment do not use a lot of real estate. This means that land used for wind turbines can often be used for other purposes, such as agriculture [25].

1.10.2 The disadvantages

- efficiency of a wind turbine to produce electricity depends on weather conditions, so it can be difficult to predict the amount of electricity a wind turbine will produce over time. If the wind speed is too low on a given day, the turbine's rotor will not turn.

- Wind energy causes noise and visual pollution: One of the main drawbacks of wind energy is noise and visual pollution. Wind turbines can be noisy when they are in operation, due to the mechanical operation and the wind vortex that is created when the blades turn. In addition, because wind turbines must be built high enough to capture a good amount of wind, they can often interrupt otherwise picturesque landscapes, such as mountain ranges, lakes, oceans, etc [25].

Chapter 2

State of the art in wind turbines

To improve the performance of Savonius wind turbine, it has several studies for a better understanding of these phenomena and their consequences. Different approaches have been performed: experimental, analytical and numerical.

In 2011, I.Dobrev and F.Massouh [26] ,They studied the flow through a Savonius type vertical axis wind turbine using CFD to study the behavior of a Savonius wind turbine under flow field conditions and to determine its performance and the evolution of the wake geometry. The flow analysis helps qualify the wind turbine design. To validate the simulations, they compared the results of the flow simulation and the calculations performed under the different conditions: 2D and 3D flow with the turbulence model kω-sst and also 3D flow with the model DES/ kω-sst with The wind tunnel experimental studies using PIV and the obtained rotor power analysis shows that the modeling results 2D/ k ω-sst are slightly higher than those of the experiments; those of the modeling 3D/ kω-sst are much lower than those of the experiments. The comparison of the wake and spill verticals with the experiment shows that the modeling 3D/ kω-sst gives similar results to the phase average velocity, but not to the actual instantaneous velocity. Furthermore, the flow structures are almost identical with respect to the rotor symmetry plane. This study shows that the best simulation of the flow is the simulation with the 3D DES/ kω-sst, which gives similar results with the experiments.

In 2014, F.Wenehenubuna , A. Saputraa , H. Sutanto [27] , they studied experimentally in wind tunnel the performance of Savonius type wind turbines in rotation with different number of blades and compared with the simulation with ANSYS13.0, they obtained the following results :
- The number of blades will influence the rotor rotation of the wind turbine models. The three-bladed wind turbine produces a higher rotational speed and point speed ratio than the two and four blade wind turbines. The highest point speed ratio is 0.555 for a wind speed of

7 m/s.

- The rotor of a four-bladed wind turbine has a high torque compared to a two or three-bladed rotor.

- Four-bladed wind turbines perform well with a lower tip speed ratio, but three-bladed wind turbines perform better with a higher tip speed ratio.

Mahmoud, N. H., El-Haroun, A. A., Wahba, E., Nasef, M. H. (2012) [28] In this thesis, different geometries of the Savonius wind turbine are studied experimentally to determine the most efficient operating parameters. It was found that the two-blade rotor is more efficient than three and four.The end-plate rotor gives higher efficiency than those without end plates. Double stage rotors perform better than single stage rotors. Rotors with no overlap ratio (β) perform better than those with overlap. The results also show that the power coefficient increases with increasing aspect ratio (α).

In 2015, TIAN, Wenlong, SONG, Baowei, VANZWIETEN, James H [29], they studied a modified Savonius wind turbine with new blade shapes is introduced with the aim of increasing the power coefficient of the turbine. The effect of blade fullness, which is one of the main blade shape parameters, on the power output of a The two-bladed Savonius wind turbine is investigated using dynamic transient computational fluid (CFD). The simulations are based on Reynolds average Navier-Stokes (RANS) equations with a turbulent renormalization group model. This numerical method is validated with existing experimental data and then used to quantify the performance of design variants, they obtained the following results :

- The rotor with a blade fullness of n = 1 has the highest power coefficient, 0.2573, which is $10,98\%$ higher than a standard Savonius turbine.

- During a rotation period, the vane with a smaller fullness generates both higher positive torque and lower negative torque values.

- Turbines with n $\leq$ 1 have larger wakes than those of n > 1.

In 2012, Driss, Z., Abid, M. S [30]. Numerical investigations were conducted to study the flow of the aerodynamic structure around the Savonius wind rotor. The CFD code "Flow-Works" was used to present the local characteristics in different transverse and longitudinal

planes of the wind tunnel. The numerical model considered is based on the solution of the Navier-Stokes equations in conjunction with the standard k-ω turbulence model. These equations have been solved by a finite volume discretization method. The comparison between the numerical results and the global experimental results, performed in an open wind tunnel, confirms the validity of the numerical method. The results confirm that the Savonius wind rotor has an effect on the local characteristics. The results of the numerical simulation, performed in the framework of the CFD code FlowWorks, are in good agreement with the experimental results. The good agreement confirms the numerical methods.

Ghosh, A., Biswas, A., Sharma, K. K., Gupta, R. (2015) [31].In this study, they attempted to investigate the unsteady aerodynamics of a three-bladed, three-bucket Savonius Rotor at low Reynolds number. The power coefficients of the combined rotor were first evaluated and the results were validated with the experimental results. The validated numerical code was then exploited to understand the physical processes responsible for its power generation in low wind conditions. The study led to the following conclusions :

-Blade-fluid interactions confirm a higher vortex concentration on the downstream side of the Darrieus rotor than on the downstream side of the Savonius rotor, which can be attributed to the Coanda effect. This effect is accompanied by a compression of the vortices downstream of the Darrieus rotor, which pushes the rotor in its rotation and thus increases the energy production.

-Presence of stall vortices on Darrieus blades and increased concentration of vortices downstream of the Darrieus rotor justifies the design of the Darrieus rotor above the Savonius rotor, which could result in a high value of the rotor power coefficient in low Reynolds number flow.

-There is a speed deficit in the downstream of the Savonius rotor compared to the Darrieus rotor for which the Darrieus rotor would be able to extract more energy by its presence on top compared to the Savonius rotor.

Kacprzak, K., Liskiewicz, G., Sobczak, K. (2013) [32], The authors have numerically analyzed three geometries of Savonius wind turbines rotors, namely the classical, Bach type and Elliptical patterns rotors. The results for the first two were compared with those of the experimental data. Then, the review focused on a comparison of the numerical results ob-

tained for each simulated rotor geometry. The main results of these actions are presented below :

-When a transition model is not applied, in the case of fluid velocities, a significant over-estimation in terms of the expected torque could occur. The source of this difference was identified and explained by a significant contribution of the laminar part of the boundary layer.

-All rotors examined reach their maximum power at a top speed ratio of 0.8.

-In the range of tip speed ratios between 0.2 and 0.4, the Savonius Elliptical Rotor outperforms the Bach type and the Savonius Classic Rotor.

This study by D.Alexander ; M.Aliferis ; J. Stette ;Tania Bracchi and R. Jason Hearst in 2018 [33] . reported measurements of the aerodynamic performance and wake evolution of a Savonius wind turbine at two Reynolds numbers and two turbulence intensities. Like Akwa et al, the results show that the power coefficient decreases with higher input TI. However, this decrease is only observable for the higher Reynolds number. Thus, the $\Re$ dependence of the power coefficient is reduced as the turbulence is increased. The drag coefficient showed a weak dependence at λ, and a slight decrease was found for higher inlet TI. This finding is also confirmed by previous CFD simulations performed by Pol. In the context of a cylinder in a high TI flow, this effect may possibly be related to a lower separation of the flows around the turbine. Finally, given the results presented in this article represents the possibility to give some indications on the optimal placement of the turbines Savonius. Due to the blocking of the incoming wind by the first rotor.

In 2020 CHENITI Dounia and ALILICHE Khawla [15].They are looking to study a vertical wind turbine of Savonius type. They had studied the wind turbines with two and three blades in order to know the wind turbine that has the best. On the other hand, they had studied the influence of the wind speed, the rotation speed on the power produced by the wind turbine. The research work was focused on the analysis of the power coefficient (C_p) of wind turbine. The work consisted in the numerical simulation of the fluid dynamics (Computation Fluid Dynamic CFD) of the wind flow around a Savonius . The results obtained proved that the increase in the number of blades, wind speed and specific speed gives the wind turbine better properties. However, an increase of the dawn radius decreases the wind turbine power.

In 2017 , ZEMAMOU, M., AGGOUR, M., et TOUMI,A , [34] conducted a study to compare several results from published papers on the performance of new Savonius rotor designs. The objective is to provide an important background for future studies on this type of wind turbine. The Savonius rotor has proven its performance due to its simple design, low cost and low starting torque at low wind speed, despite its low efficiency due to the negative torque applied to the return blade, research aims to improve the design of the Savonius rotor in order to achieve better performance. According to the results of this review, they conclude that over the years, the development of the Savonius rotor blade shape remains a very promising area of research in order to improve the performance of the rotor, It is perceived that research on parameters such as AR, overlap ratio and number of blade can be further studied to achieve a satisfactory level of performance.

In 2014, GAD, H. E., ABD EL-HAMID, A. A., EL-ASKARY, W. A., and al. [35] have numerically realized a modified Savonius wind rotor by focusing on the average torque and power coefficients over a full operating cycle. The numerical study is performed using the commercial software Fluent 6.3.26 with four different turbulence models. The calculations are tested against the available experimental data in order to select the appropriate turbulence model and thus extend the numerical investigation. The conservation of mass and momentum equations are solved by the finite volume method. The SST turbulence model k-ω is used because of its good agreement with published works. The results showed that the modification of the rotor blades leads to an increase in rotor performance. One of the newly developed polynomial blade shapes has the highest values of average torque and average power coefficients compared to the other shapes.

In 2019 ,BAI, H. L., CHAN, Chun Man, ZHU, X. M., et al. [36] They study the performance of a Savonius vertical axis wind turbine (VAWT) placed in a long confined channel, based on computational fluid dynamics (CFD) simulations. The two-dimensional (2D) simulations are performed with ANSYS Fluent, using the turbulence model k-ω shear stress transport (SST). The incoming wind speed at the channel entrance is Uo = 4,05 m/s, which corresponds to a Reynolds number $\Re$ =$1, 0 \times 10^5$, based on Uo and the diameter (D) of the wind turbine. The channel has a length of 45D. Three different widths, 2D, 3D and 4D, of the channel as well as different locations of the wind turbine in the channel are considered. The results show

that the power output (Pout) of the Savonius-type VAWT turbine placed in the channel can be increased by 200% in the two-dimensional wide channel compared to that in the open space. In addition, a higher optimal peak speed ratio (TSR) is observed for the wind turbine located in the channel than in open space.

In 2010 ,D'ALESSANDRO, V., MONTELPARE, S., RICCI, R., and al [37], studied the complex flow field that develops around a Savonius wind rotor and evaluated its performance. A mathematical model of the interaction between the flow field and the rotor blades was developed and validated by comparing its results with data obtained at the Environmental Wind Tunnel (EWT) of the Polytechnic University of Marche. The rotor blades were treated as rigid bodies and their behavior was modeled using the second cardinal equation of dynamics. The experimental data were used to validate the developed computational methodology. The comparison of the performance data obtained by the numerical simulations and the experimental measurements shows a very good agreement. This suggests the use of this numerical method for the study of new blade shapes in order to produce better rotor performance. The results presented by numerical simulations provided insight into the average characteristics of the flow field.

In 2013, ALI, Mohammed Hadi [38] , conducted an experimental comparison to study the performance and make a comparison between a two and three blade Savonius wind turbine. These two models were tested and studied using a subsonic wind tunnel that was built for this purpose under low wind speed due to several reasons, including that the Savonius wind turbine has its maximum performance at (λ = TSR = 1) and high starting torque at low wind speeds. It was observed from the measured and calculated results that the two-bladed Savonius wind turbine is more efficient, it has a higher power coefficient under the same test conditions than the three-bladed Savonius wind turbine. The reason is that increasing the number of blades will increase the The reason is that increasing the number of blades will increase the drag surfaces against the wind airflow and cause the reverse torque to increase and lead to the decrease of the net torque working on the blades of the Savonius wind turbine.

In 2004,MENET, Jean-Luc et BOURABAA, Nachida [39] Have made a study to use a two-stage Savonius rotor with two vanes and two end plates. The height of the rotor should be twice its diameter. The primary overlap rate should be between 0.15 and 0.3 times the vane diameter, while the secondary overlap rate should be equal to 0. The results of the simulation propose the optimal values for the geometrical parameters. This simulation allows not only to specify the nature of the flow, but also to determine the aerodynamic behavior of the rotor. The results are compared to the experimental data. The influence of a central shaft and Reynolds number is studied, as well as the presence and geometry of an external frame. These considerations allow to define an optimal geometrical configuration.

Conclusion Our thesis aimed to study the aerodynamic performance of a two-bladed Savonius airfoil, the calculations are performed using a computational fluid dynamics code CFD and OpenFoam based on the finite volume method .

Chapter 3

Aerodynamics of Wind Turbines

3.1 Introduction

The design of wind turbines starts with the knowledge of the aerodynamic forces acting on the turbine. The energy output of a wind turbine is therefore dependent on the interaction between the rotor and the wind. The main aspects of the performance of a wind turbine, such as power production and loads, are therefore determined by the aerodynamic forces generated by the wind. These can only be understood with a thorough understanding of the aerodynamics of steady state operation.

3.2 Energy provided by the wind

3.2.1 Kinetic energy

Wind turbines work by converting the kinetic energy of the wind into rotational kinetic energy in the turbine, and then into electrical energy that can be supplied. The kinetic energy is :

$$E_c = \frac{1}{2}mV^2 \tag{3.1}$$

- V : the wind velocity (m/s).

- m : The density of the air, i.e. the weight of the air in (kg).

- E_c: kinetic energy (in joules).

3.2.2 Mass of the air

At normal atmospheric pressure, temperature of 15 degrees Celsius the air has a density of about 1,225 (kg/m^3) .However, it should be noted that the density of humid air is lower than

that of dry air.

$$m = \rho V_0 \tag{3.2}$$

m : mass of the air volume (kg) .

V_0 : occupied air volume (m^3).

ρ: density (kg/m^3).

3.3 Theoretically recoverable energy

3.3.1 Instantaneous wind power

The wind turbine is a machine capable of converting the kinetic energy of the wind into mechanical energy. The mechanical energy is then converted into electrical energy by a wind generator. The instantaneous power of the wind is given by the relation :

$$P_{wind} = \frac{1}{2}\rho A V^3 \tag{3.3}$$

P_{wind}:power of the wind incidence (W).

ρ :Density ($kg/m3$).

A : projected area of the rotor (m^2).

V : velocity of the wind incidence (m/s).

3.3.2 Betz's theory

The fundamental theory of wind turbine design and operation is derived from an approach based on the first principles of conservation of mass and conservation of energy in a wind flow. This fundamental equation was first introduced by the German engineer Albert Betz in 1919 and published in his book "Wind Energy and its Extraction through Wind Mills" in 1926 [40], The theory developed applies to both VAWT and HAWT. Betz developed the global theory of wind machines according to which the wind rotor is assumed to be an ideal energy converter, which means that :

- It does not have a hub (hub).

- It has an infinite number of rotor blades that cause no resistance to the wind passing through them.

The limited efficiency of a wind turbine is due to the braking of the wind from its upstream speed V_1 at its downstream speed V_2, while allowing the flow regime to continue. The additional losses in efficiency of a wind turbine are caused by viscous and pressure drag on the rotor blades. If we consider the ideal model shown in Figure(3.1)[40], the section swept by the turbine blade is given by S, the section of air upwind of the rotor is given by S_1, and to the wind by S_2. The wind speed through the turbine rotor is considered uniform as V, with its value as V_1 upwind, and as V_2 downwind at a distance from the rotor. The extraction of mechanical energy by the rotor is done by reducing the kinetic energy of the air flow from upstream to downstream, or by simply applying a braking action on the wind.
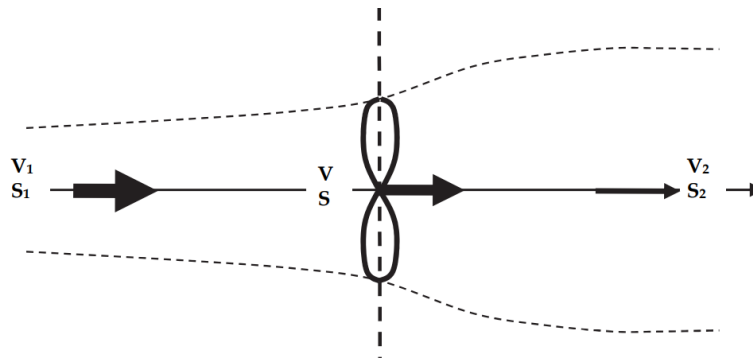
This implies that : $V_2 \prec V_1$

Figure 3.1: Flow through a wind turbine

As a result, the cross-sectional area of the airflow increases from the upstream of the turbine to the downstream location, and : $S_2 \succ S_1$

If the air flow is considered as an incompressible flow, the conservation of mass or the continuity equation can be written as follows :

$$\dot{m} = \rho S_1 V_1 = \rho S V = \rho S_2 V_2 = constant \tag{3.4}$$

This expresses the fact that the mass flow rate is a constant along the wind flow. Continuing

with the derivation, Euler's theorem gives the force exerted by the wind on the rotor as :

$$F = ma$$
$$= m\frac{dV}{dt}$$
$$= \dot{m}\Delta V$$

$$F = \rho S V(V_1 - V_2) \tag{3.5}$$

The differential energy or differential work done in the wind stream is given by :

$$dE = Fdx \tag{3.6}$$

The energy content of the wind flow :

$$P = \frac{dE}{dt} = F\frac{dx}{dt} = FV \tag{3.7}$$

By substituting the force F in the equation (3.5), we obtain the extractable power of the wind:

$$P = \rho S V^2(V_1 - V_2) \tag{3.8}$$

The power as the rate of change of kinetic energy from upstream to downstream is given by:

$$P = \frac{\Delta E}{\Delta t}$$
$$= \frac{\frac{1}{2}mV_1^2 - \frac{1}{2}mV_2^2}{\Delta t}$$

$$= \frac{1}{2}\dot{m}(V_1^2 - V_2^2) \tag{3.9}$$

Using the continuity equation (3.4), we can write :

$$P = \frac{1}{2}\rho S V(V_1^2 - V_2^2) \tag{3.10}$$

By putting the two expressions of the power P in the equations(3.8) and (3.10), we obtain :

$$P = \frac{1}{2}\rho S V(V_1^2 - V_2^2) = \rho S V^2(V_1 - V_2) \tag{3.11}$$

The last expression implies that :

$$\tfrac{1}{2}(V_1^2 - V_2^2) = \tfrac{1}{2}(V_1 - V_2)(V_1 + V_2)$$
$$= V(V_1 - V_2), \forall V, S, \rho \neq 0$$

or:

$$V = \frac{1}{2}(V_1 + V_2), \forall (V_1 - V_2) \neq 0; or V_1 \neq V_2 \tag{3.12}$$

This in turn suggests that the wind speed at the rotor can be considered as the average of the upstream and downstream wind speeds. This also implies that the turbine must act as a brake, reducing the wind speed from V_1 to V_2, but without reducing it totally to V = 0, at which point the equation is no longer valid. To extract energy from the wind stream, its flow must be maintained and not totally stopped. The last result allows us to write new expressions for the force F and the power P as a function of the upstream and downstream speeds by substituting the value of V as :

$$F = \rho SV(V_1 - V_2) = \frac{1}{2}\rho S(V_1^2 - V_2^2) \tag{3.13}$$

$$\begin{aligned} P &= \rho SV^2(V_1 - V_2) \\ &= \tfrac{1}{4}\rho S(V_1 + V_2)^2(V_1 - V_2) \\ &= \frac{1}{4}\rho S(V_1^2 - V_2^2)(V_1 + V_2) \end{aligned} \tag{3.14}$$

We can introduce the "downstream velocity factor," or "interference factor," b as the ratio of the downstream speed V_2 to the upstream speed V_1 as :

$$b = \frac{V_2}{V_1} \tag{3.15}$$

From the equation (3.13), the force F can be expressed as :

$$F = \frac{1}{2}\rho SV_1^2(1 - b^2) \tag{3.16}$$

The extractable power P in terms of the interference factor b can be expressed as :

$$P = \frac{1}{4}\rho S(V_1^2 - V_2^2)(V_1 + V_2) = \frac{1}{4}\rho SV_1^3(1 - b^2)(1 + b) \tag{3.17}$$

The kinetic power content of the undisturbed upstream wind stream with V = V_1 and over a cross sectional area S becomes :

$$P_{wind} = \frac{1}{2}\rho SV_1^3, \left[\frac{joules}{m^2.s}m^2\right], [Watts] \tag{3.18}$$

The power coefficient or efficiency is the dimensionless ratio between the power available in the wind and the power developed by the rotor.

$$C_p = \frac{P}{P_{wind}} \tag{3.19}$$

By substituting the expressions for P from the equation (3.17) and for Pw of the equation (3.18), we have :

$$C_p = \frac{P}{P_{wind}} = \frac{\frac{1}{4}\rho S V_1^3 (1-b^2)(1+b)}{\frac{1}{2}\rho S V_1^3}$$

$$= \frac{1}{2}(1-b^2)(1+b) \tag{3.20}$$

When b = 1, $V_1 = V_2$ and the windstream is undisturbed, leading to a performance coefficient of zero. When b = 0, $V_1 = 0$, the turbine stops all the air flow and the performance coefficient is equal to 0,5. We can notice on the graph figure(3.2) [40] that the power coefficient reaches a maximum around b =1/3
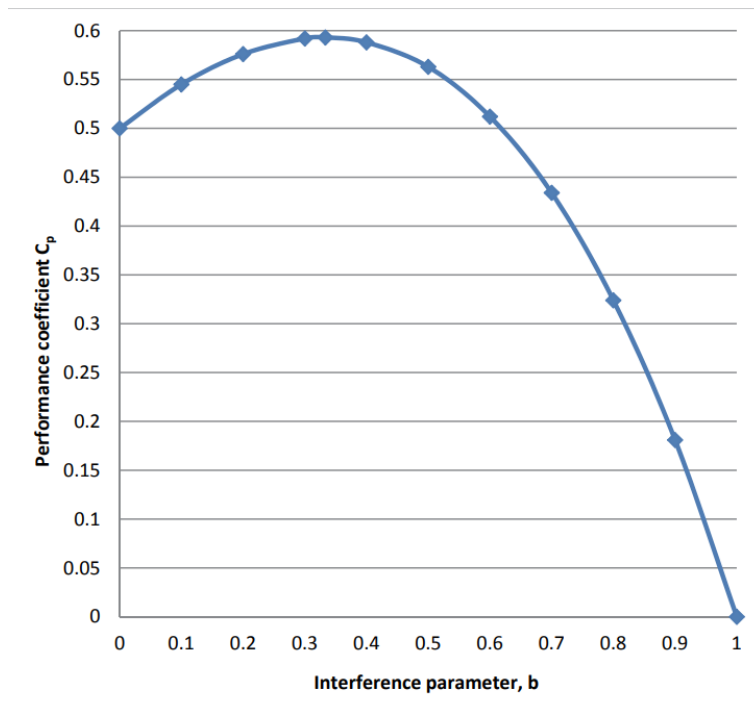

Figure 3.2: The power coefficient C_p as a function of the interference factor b

Maximum performance can be obtained by differentiating the equation (3.20) with respect to the interference factor b, and setting the derivative equal to zero, we obtain :

$$\frac{d}{dx}(uv) = u\frac{dv}{dx} + v\frac{du}{dx}$$
$$\frac{dC_p}{db} = \frac{1}{2}\frac{d}{db}[(1-b^2)(1+b)]$$
$$= \frac{1}{2}[(1-b^2) - 2b(1+b)]$$
$$= \frac{1}{2}(1-b^2 - 2b - 2b^2)$$
$$= \frac{1}{2}(1-3b^2 - 2b)$$

$$= \frac{1}{2}(1-3b)(1+b) = 0 \tag{3.21}$$

40

The equation (3.21) has two solutions, the first is the trivial solution :

$$(1 + b) = 0$$

$$b = \frac{V_2}{V_1} = -1 \Rightarrow V_2 = -V_1 \tag{3.22}$$

The second solution is the practical physical solution :

$$(1 - 3b) = 0$$

$$b = \frac{V_2}{V_1} = \frac{1}{3} \Rightarrow V_2 = \frac{1}{3}V_1 \tag{3.23}$$

The equation (3.22) shows that for optimal operation, the downstream speed V_2 must be equal to one third of the upstream speed V1. Using the equation (3.20), the maximum or optimum value of the power coefficient C_p becomes :

$$C_{p,opt} = \frac{1}{2}(1 - b^2)(1 + b) = \frac{1}{2}(1 - (\frac{1}{3})^2)(1 + \frac{1}{3}) = \frac{16}{27} = 0.59259 = 59.26\% \tag{3.24}$$

The value of the Betz coefficient suggests that a wind turbine can extract at most 59,3 % of the energy of an undisturbed wind flow.

$$Betz coefficient = \frac{16}{27} = 0.592593 = 59.26\% \tag{3.25}$$

3.3.3 Mechanical torque

$$Q = \frac{P}{\omega} \tag{3.26}$$

Q:mechanical torque produced by the wind turbine(in N·m).

P:mechanical power (in W).

ω:rotation speed of rotor in (rad/s).

3.4 Specific speed (TSR)

TSR is the ratio of blade tip rotation speed and the real wind speed and is described as lambdaλ. Is a factor that directly affects the energy generated by the turbine. Its expression is given by the following relation :

$$\lambda = TSR = \frac{\omega R}{V} \tag{3.27}$$

ω:rotation speed of rotor in (rad/s).

R:radius of the rotor in meters (m).

V : velocity of the wind incidence (m/s).

The TSR determines the rotational speed of the wind turbine is usually dependent on the particular design of the wind turbine used. If the rotor spins too fast, it appears to the wind as a large flat disk, which creates a large amount of drag. The rotor Tip Speed Ratio, TSR, depends on the blade profile used, the number of blades and the type of turbine. With
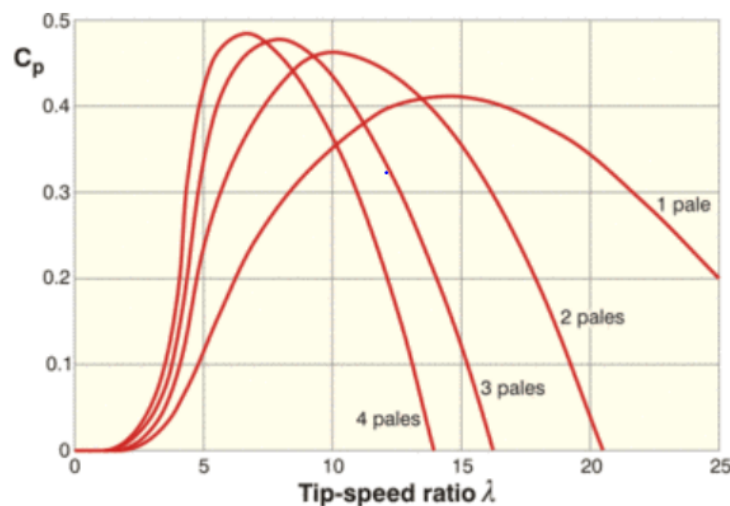

Figure 3.3: Evolution of the aerodynamic efficiency as a function of the number of blades

regard to the above figure 3.3[41], which shows the evolution of the aerodynamic efficiency as a function of the number of blades for a given model, we can see that the more the number of blades is important, the lower the optimal speed ratio at the tip of the blade is low. In addition, the analysis of the performance of several wind turbines shows that there is a clear trend towards better performance for Wind turbines with lower rated wind speeds between 10 m/s et 12 m/s.

3.5   The wake generated by a wind turbine

The wind wake is a turbulent structure that emanates from the rotating rotor blades. Then this turbulent structure evolves downstream of the wind rotor and forms marginal turbulence. The wake has two domains: the near wake and the far wake. The near wake plays an important role in the evaluation of the aerodynamic performance of the wind rotor. In addition, it

allows to define the initial conditions for the development of the far wake. Understanding the latter allows to improve the design of wind farms by minimizing interactions between wind turbines.[42]

The wake structure downstream of a wind turbine can be revealed by the presence of smoke in the air passing through the rotor. The figure 3.4[43] shows the wake and the marginal turbulence revealed by smoke in wind tunnel.

The figure 3.5[43] taken in 1997 by the National Laboratory of Risoe shows the close wake revealed by the smoke in real conditions.

Figure 3.4: Visualization of the wake by the smoke in a wind tunnel

Figure 3.5: Wake structure downstream of a wind turbine, revealed by smoke; Risoe1997

3.6 Wake structure

The vortex system of a horizontal axis wind turbine consists of a vortex sheet emanating from the trailing edge and marginal vortices emanating from the blade tips. These vortex

structures have a helical motion and move downstream of the rotor. In addition, marginal vortices originate at the hub and then move mainly in a linear path along the axis of rotation. The Figure 3.6 [42] illustrates schematically the marginal vortices emitted by a wind rotor.
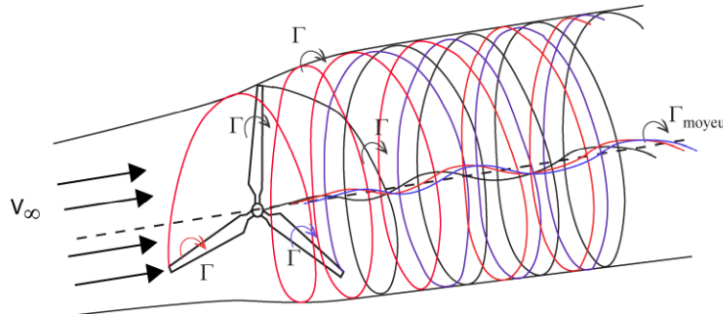

Figure 3.6: Schematic drawing of the vortex system behind a wind turbine

3.7 The characteristics of a wind turbine's wake

For a wind turbine placed in a uniform flow, the wake is composed of three distinct regions: the near wake, the transition zone and the far wake. The near wake is characterized by strong pressure and velocity gradients and by an increase in the turbulence level, which will result, for another wind turbine located in this wake zone, in a decrease in power and an increase in aerodynamic loads on the rotor. After this zone, the turbulence generated by the wind turbine gradually degrades and only the effects of shear and atmospheric turbulence figure 3.7[43].
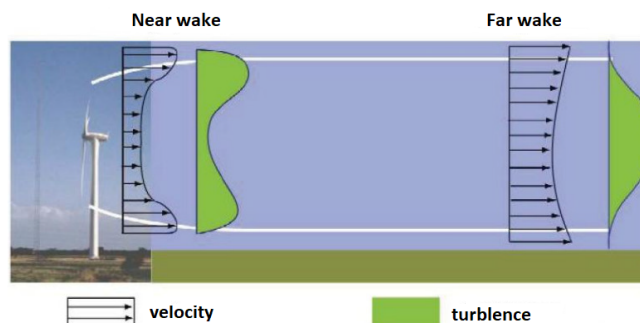

Figure 3.7: Near and far wakes

3.8   Rotor Savonius

3.8.1   Functional principle

The Savonius turbine was invented by the Finnish engineer Sigurd Johannes Savonius in 1922 and is classified as a drag type machine, as the incoming wind "causes" the blade to rotate around its vertical axis, the drag force caused by the incoming wind actually acts on both sides of the rotor blade, however, the force on the convex side is higher than the force on the concave side, which creates a net force that drives the rotor.Figure 3.8[44]
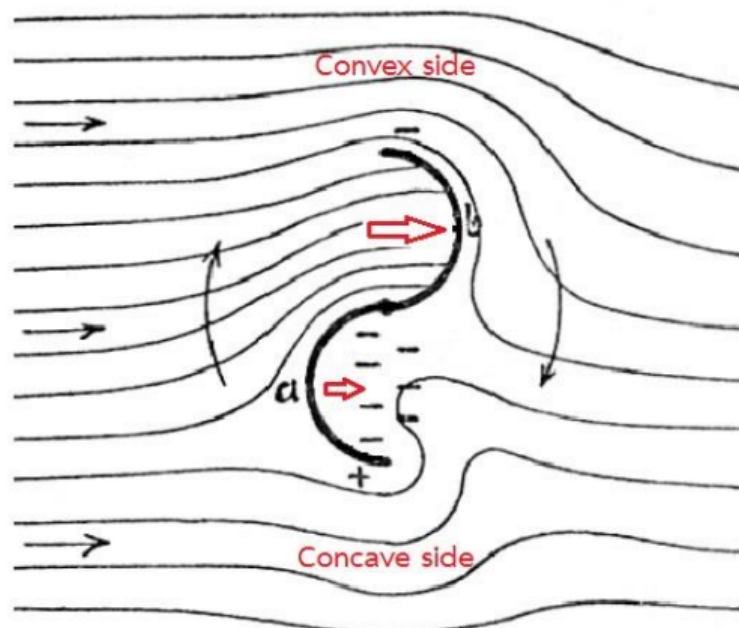

Figure 3.8: Net force acting on the Savonius blade

3.8.2   Design parameters

Several researches[45][39][27]studies were carried out on the performance of the Savonius rotor based on different geometric configurations of its rotor. These studies were carried out on the basis of a numerical analysis of calculation using CFD (Computational Fluids Dynamics) and experimental tests in wind tunnel. The different configurations that have been developed have sought to improve the performance of the aerodynamic behavior of the Savonius rotor.This is why the geometric configuration is fundamental in terms of performance, The configuration for a Savonius rotor is determined by the following rotor design

parameters :

- Rotor aspect ratio.

- Surface swept by the rotor blades.

- Geometric shape of the blades (profile, chord length).

- Ratio of overlap and blade spacing.

- Number of blades and stages.

The geometrical shape of the blades will be semi-circular, keeping the the traditional Savonius rotor blade shape.Figure3.9 [39]shows the profile with its dimensions. The overlap
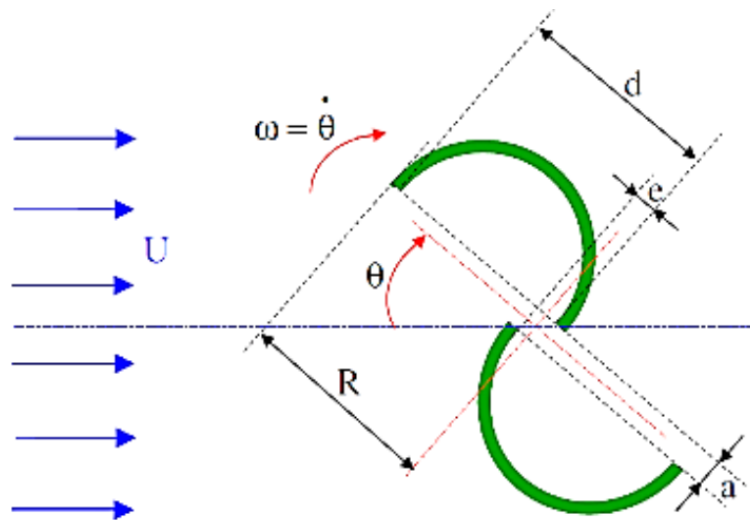

Figure 3.9: Schematic of a Savonius rotor

relation is a dimensionless parameter that relates the gap distance of the half-cylinders and diameter of a half-cylinder, which is given as follows :

$$overlap relation = R_s = \frac{e}{d} \tag{3.28}$$

3.8.3 Coefficient of moment

The coefficients used for the moment are similar to the lift, drag and thrust coefficients, and are also dimensionless.

$$C_m = \frac{M}{\frac{1}{2}\rho A R V^2}$$

C_m: Coefficient of moment.

M:Moment $(N.m)$.

A: projected area of the rotor m^2.

R :radius of the rotor in meters (m).

V: wind velocity (m/s).

ρ: Density (kg/m^3).

3.8.4 Coefficient of lift and drag

there are two types of aerodynamic forces, lift and drag. Consequently, there are two non-dimensional parameters. The formula for lift is given below, the formula for drag is given after:

$$C_L = \frac{F_L}{\frac{1}{2}\rho AV^2}$$

$$C_D = \frac{F_D}{\frac{1}{2}\rho AV^2}$$

F_D: drag (N).

F_L: lift (N).

ρ: Density (kg/m^3).

A: projected area of the rotor m^2.

V: wind velocity (m/s).

Chapter 4

Mathematical and Numerical Modeling of the problem

4.1   Introduction

Mathematical modeling and numerical solution are the essential parts in the numerical simulation of the studied problem. The flow in the rotor of a vertical axis wind turbine of Savonius type is considered in the framework of Navier-Stokes equations in the two-dimensional formulation, solving balance equations translating two fundamental principles: : conservation of mass and the quantity of motion.

4.2   Mathematical modeling

The numerical prediction of fluid flows is based on the resolution of balance equations translating two fundamental principles : conservation of mass and the fundamental principle of dynamics.

4.2.1   Navier Stocks equations

The conservation of mass equation

$$\frac{\partial \rho}{\partial t} + \frac{\partial}{\partial x_i}(\rho u_i) = 0 \tag{4.1}$$

For a simple formulation of the problem, we will assume that the flow is incompressible :
ρ=cst

So for a 2D flow, the equation (4.1) becomes in the following form:

$$\frac{\partial U_i}{\partial x_i} = 0 \tag{4.2}$$

The conservation equation of the quantity of motion[46]   By applying the fundamental principle of dynamics stated by Newton and assuming incompressible flow we have :

$$\frac{\partial U_i}{\partial t} + \frac{\partial}{\partial x_i}(u_i u_j) = -\frac{1}{\rho}\frac{\partial \rho}{\partial x_i} + \frac{\partial}{\partial x_j}(\mu \frac{\partial U_i}{\partial x_i})$$ (4.3)

Knowing that :

$$\frac{\partial}{\partial x_i}(u_i u_j) = u_i \frac{\partial u_j}{\partial u_j} + u_j \frac{\partial u_i}{\partial u_j}$$

And according to the equation (4.1) :

$$\frac{\partial u_j}{\partial u_j} = 0$$

Then:

$$\frac{\partial}{\partial x_i}(u_i u_j) = u_j \frac{\partial u_i}{\partial u_j}$$

The equation (4.3) can be written as :

$$\frac{\partial U_i}{\partial t} + u_j \frac{\partial u_i}{\partial u_j} = -\frac{1}{\rho}\frac{\partial \rho}{\partial x_i} + \frac{\partial}{\partial x_j}(\mu \frac{\partial U_i}{\partial x_i})$$ (4.4)

When the flow is turbulent, it is possible to decompose any vector or scalar quantity into an average part and a fluctuating part. This is the Reynolds decomposition, presented by the following equation :

$$\phi = \bar{\phi} + \phi'$$ (4.5)

Or: $\bar{\phi}$ is the average of ϕ and ϕ' is the fluctuation.

It is by applying the Reynolds decomposition on the conservation of mass equations and conservation of motion quantity, that we obtain the following system of equations which represents the RANS expressions :

$$\frac{\partial \bar{u}_i}{\partial x_i} = 0$$ (4.6)

$$\frac{\partial \bar{u}_i}{\partial t} + \frac{\partial \bar{u}_i}{\partial x_j} = -\frac{1}{\rho}\frac{\partial \bar{p}}{\partial x_i} + v\frac{\partial^2 \bar{u}_i}{\partial x_i \partial x_j} - \frac{\partial \overline{u_i' u_j'}}{\partial x_j}$$ (4.7)

The projection of the equations (4.6) and (4.7) on the x and y axis gives us :

$$\frac{\partial \bar{u}}{\partial x} + \frac{\partial \bar{v}}{\partial y} = 0$$ (4.8)

$$\bar{u}\frac{\partial \bar{u}}{\partial x} + \bar{u}\frac{\partial \bar{u}}{\partial y} = -\frac{1}{\rho}\frac{\partial \bar{p}}{\partial x} + v(\frac{\partial^2 \bar{u}}{\partial x^2} + \frac{\partial^2 \bar{u}}{\partial y^2}) + (-\frac{\partial \overline{u'^2}}{\partial x} - \frac{\partial \overline{u'v'}}{\partial y})$$ (4.9)

$$\bar{u}\frac{\partial \bar{v}}{\partial x} + \bar{u}\frac{\partial \bar{v}}{\partial y} = -\frac{1}{\rho}\frac{\partial \bar{p}}{\partial x} + v(\frac{\partial^2 \bar{v}}{\partial x^2} + \frac{\partial^2 \bar{v}}{\partial y^2}) + (-\frac{\partial \overline{v'^2}}{\partial x} - \frac{\partial \overline{u'v'}}{\partial y})$$ (4.10)

The term $\frac{\partial \overline{u'_i u'_j}}{\partial x_j}$ s called the Reynolds Tensor, it represents the turbulent correlations, it introduces 6 additional unknowns to the system which makes that the system becomes with 4 equations only for 10 unknowns, it is thus necessary to close it by other equations by using a turbulence model which is appropriate to our problem.

4.3 Turbulence model

The k-omega turbulence model (k-ω) is one of the most commonly used models to capture the effect of turbulent flow conditions. It belongs to the family of RANS (Reynolds-averaged Navier-Stokes) turbulence models where all turbulence effects are modeled. The model which is the most recommended for boundary layer simulations and which gives the most accurate results is the SST model K-ω.

The model k-ω SST (Shear Stress Transport), uses the model k-ω in the near-wall zone and the k-epsilon model in the far wall zones with high Reynolds number. The SST formulation changes to a behavior k-ϵ in the free flow, which avoids the problem k-ω to be sensitive to the turbulence properties of the free flow at the inlet.

The model k-ω SST provides a better prediction of flow separation than most RANS models and also explains its good behavior in unfavorable pressure gradients. It has the ability to account for principal shear stress transport in boundary layers with unfavorable pressure gradients. It is the most commonly used model in the industry because of its high accuracy.

4.3.1 Turbulent kinetic energy

Knowing that the expression of the Reynolds tensor is given by:

$$\tau_{ij} = \rho \overline{u'_i u'_j} = \mu_t (\frac{\partial \bar{u}_i}{\partial x_j} + \frac{\partial \bar{u}_i}{\partial x_j}) \frac{2}{3} \rho k \delta_{ij} \qquad (4.11)$$

with:

δ_{ij}:is the Kronecker delta.

μ_t:is the turbulent viscosity.

We take the trace of the Reynolds tensor $\tau_{ij} = \tau_{xx} + \tau_{yy} + \tau_{zz}$ we obtain:

$$\rho(\bar{u}'^2 + \bar{v}'^2 + \bar{w}'^2) = 2\mu_t \left[\frac{\partial u}{\partial x} + \frac{\partial v}{\partial y} + \frac{\partial w}{\partial z} \right] 3(\frac{2}{3}\rho k) \qquad (4.12)$$

According to the continuity equation:

$$\frac{\partial u}{\partial x} + \frac{\partial v}{\partial y} + \frac{\partial w}{\partial z} = 0$$

The equation (4.12) becomes :

$$\rho(\bar{u'}^2 + \bar{v'}^2 + \bar{w'}^2) = 2\rho k \tag{4.13}$$

Now we can obtain the expression of the turbulent kinetic energy k :

$$k = \frac{1}{2}\bar{u'_i u'_j} = \frac{1}{2}(\bar{u'}^2 + \bar{v'}^2 + \bar{w'}^2) \tag{4.14}$$

4.3.2 The K-epsilon model (K-epsilon)

The K-epsilon model is one of the most common turbulence models. It is a two-equation model, meaning that it includes two additional transport equations to represent the turbulent properties of the flow. This allows a two-equation model to account for history effects such as convection and diffusion of turbulent energy.

the turbulent viscosity is given by the expression:

$$\mu_t = \rho C_\mu \frac{k^2}{\epsilon} \tag{4.15}$$

Then, by combining the turbulent kinetic energy and the dissipation rate, we write:

$$\bar{\epsilon} = v \frac{\partial \bar{u'_i}}{\partial x_j} \frac{\partial \bar{u'_i}}{\partial x_j} \tag{4.16}$$

Both estimated by their transport equation:

$$\frac{\partial(\rho \bar{k})}{\partial t} + \bar{u}_j \frac{\partial(\rho \bar{k})}{\partial x_j} = \frac{\partial}{\partial x_j}\left[(\mu + \frac{\mu_t}{\sigma_k})\frac{\partial \bar{k}}{\partial x_j}\right] + P_k - \rho\bar{\epsilon}$$

$$\frac{\partial(\rho \bar{\epsilon})}{\partial t} + \frac{\partial(\rho u_i \bar{\epsilon})}{\partial x_i} = \frac{\partial}{\partial x_j}\left[(\mu + \frac{\mu_t}{\sigma_\epsilon})\frac{\partial \bar{\epsilon}}{\partial x_j}\right] + \frac{\bar{\epsilon}}{k}(C_{1\epsilon}P_k - C_{2\epsilon}\rho\bar{\epsilon}) \tag{4.18}$$

The constants involved in this model have been determined in the following reference configurations :

C_μ=0.09 Logarithmic law in wall.

$C_{1\epsilon}$ =1.44 Uniform deformation or shear.

$C_{2\epsilon}$ =1.92 Isotropic turbulent growth.

σ_k=1 Comparison with jet-wake experiment.

σ_ϵ=1.3 Comparison with jet-wake experiment.

4.3.3 The K-omega model

The turbulence model K-ω is a two-equation model that uses two partial differential equations with two variables of K and ω, the first variable being the kinetic energy of the turbulence (k) while the second (ω) is the specific dissipation rate (of the kinetic energy of the turbulence k into internal thermal energy).

The turbulent frequency:

$$\epsilon = \beta \omega k \tag{4.19}$$

Turbulent viscosity :

$$\mu_t = \rho \frac{k}{\omega} \tag{4.20}$$

Turbulent kinetic energy transport :

$$\rho \frac{\partial k}{t} + \rho u_j \frac{\partial k}{x_j} = \tau_{ij} \frac{\partial u_i}{x_j} \rho \beta \omega k + \frac{\partial}{x_j} \left[(\mu + \mu_t \sigma_{k1}) \frac{\partial k}{x_j} \right] \tag{4.21}$$

The transport of the turbulent frequency :

$$\rho \frac{\partial \omega}{t} + \rho u_j \frac{\partial \omega}{x_j} = \alpha \frac{\omega}{k} \tau_{ij} \frac{\partial u_i}{x_j} \rho \beta \omega^2 + \frac{\partial}{x_j} \left[(\mu + \mu_t \sigma_{\omega 1}) \frac{\partial \epsilon}{x_j} \right] \tag{4.22}$$

with:

α=0.5

β=0.075

β=0.09

σ_{k1}=2

$\sigma_{\omega 1}$=2

4.3.4 The K-omega SST model

The SST k-omega turbulence model is a two-equation turbulence model that is used for many aerodynamic applications. It is a hybrid model combining the Wilcox k-omega model and the k-epsilon model. A mixing function, F_1, activates the Wilcox model near the wall and the k-epsilon model in the free flow. This ensures that the appropriate model is used in the entire flow field :

- The k-omega model is well adapted to the simulation of the flow in the viscous sub-layer.

-The k-epsilon model is ideal for predicting the flow behavior in regions far from the wall.Ou

$F_1 = 1$ to the wall and F_1=0 away from the wall.

Turbulent kinetic energy transport :

$$\rho\frac{\partial k}{t} + \rho u_j \frac{\partial k}{x_j} = \tau_{ij}\frac{\partial u_i}{x_j}\rho\beta\omega k + \frac{\partial}{x_j}\left[(\mu + \mu_t\sigma_{k3})\frac{\partial k}{x_j}\right]$$
(4.23)

The transport of the turbulent frequency :

$$\rho\frac{\partial\omega}{t} + \rho u_j \frac{\partial\omega}{x_j} = \frac{\alpha_3}{v_t}\tau_{ij}\frac{\partial u_i}{x_j}\rho\beta_3\omega^2 + \frac{\partial}{x_j}\left[(\mu + \mu_t\sigma_{\omega3})\frac{\partial\epsilon}{x_j}\right] + 2\rho(1 - F_1)\sigma_{\omega2}\frac{1}{\omega}\frac{\partial k}{\partial x_j}\frac{\partial\omega}{\partial x_j}$$
(4.24)

4.3.5   Wall functions

The wall function is used to bridge the gap between the interior region of the wall and the region of fully developed turbulence, and is used to determine the boundary conditions in the near-wall region. One of the most important parameters important to judge the applicability of wall function is the distance a dimensional to the wall Y+ is given by the expression :

$$Y+ = \frac{YU_T}{\nu}$$
(4.25)

$$U_T = \sqrt{\frac{\tau_W}{\rho}}$$
(4.26)

with:

U_T :the speed of friction.

τ_W: the shear stress .

Y:the absolute distance from the wall.

ν:kinematic viscosity (m^2/s).

The near wall region is divided into three regions which means that three sub layers can be clearly identified:

-Viscous sub-layer (0 <y+< 5) near the wall, where viscous effects dominate the flow and the velocity profile is clearly linear :

$$u^+ = y^+$$

-The buffer layer (5 < y+ < 30) between sublayers, where the velocity profile changes from linear to logarithmic and where no clear law can be observed.

-The logarithmic zone (y+ > 30) in the logarithmic layer, turbulence stresses dominate the flow and the velocity profile varies very slowly with a logarithmic function along the distance y.

$$u^+ = \frac{1}{\kappa}\ln(y^+) + B$$

κ:t the VonKarmen constant κ=0.41.

B: is a parameter that varies according to the roughness of the wall.

4.4 Numerical modelling

Before carrying out the simulation of an airflow around a two-bladed savonius rotor, different programs are used to obtain the best result (gambit, openfoam, qtiplot), the first step is to define the geometry using Gambit, then we divide the geometry in two parts : the rotor (Savonius wind turbine) and the stator (calculation area). We make the mesh of each part, then with openfoam, we merged the two parts of the geometry and we define the boundary conditions at the borders of the calculation domain and with qtiplot we show the result obtained. To carry out the study we put these objectives :

- Creation of geometry and calculation area.

- Discretization of the calculation domain.

- The calculation with OpenFoam.

- Viewing and comparing results.

4.4.1 Gambit

GAMBIT is a geometry and mesh generation software for computational fluid dynamics (CFD) analysis. GAMBIT has a unique interface for geometry and mesh creation that brings together several pre-processing technologies in a single environment. figure 4.1
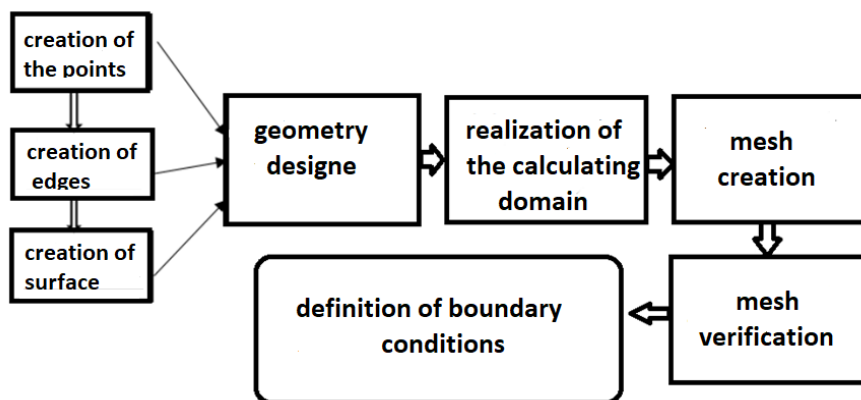
Figure 4.1: gambit operating structure

4.4.2 Geometry and mesh

Using the software gambit, we realized the two geometries in 2D according to the coordinates (x,y), the geometries are the rotor and the stator. The geometry of the rotor is in the form of two semicircular blades of small thickness. The blades are spaced from each other by a distance "e" and diameter "D" with a circle of diameter "D_0" which includes the two blades figure 4.2 . The dimensions of the rotor are :

-D=0.219 m.

-D_0=0.6 m.

-e=0.0115 m.
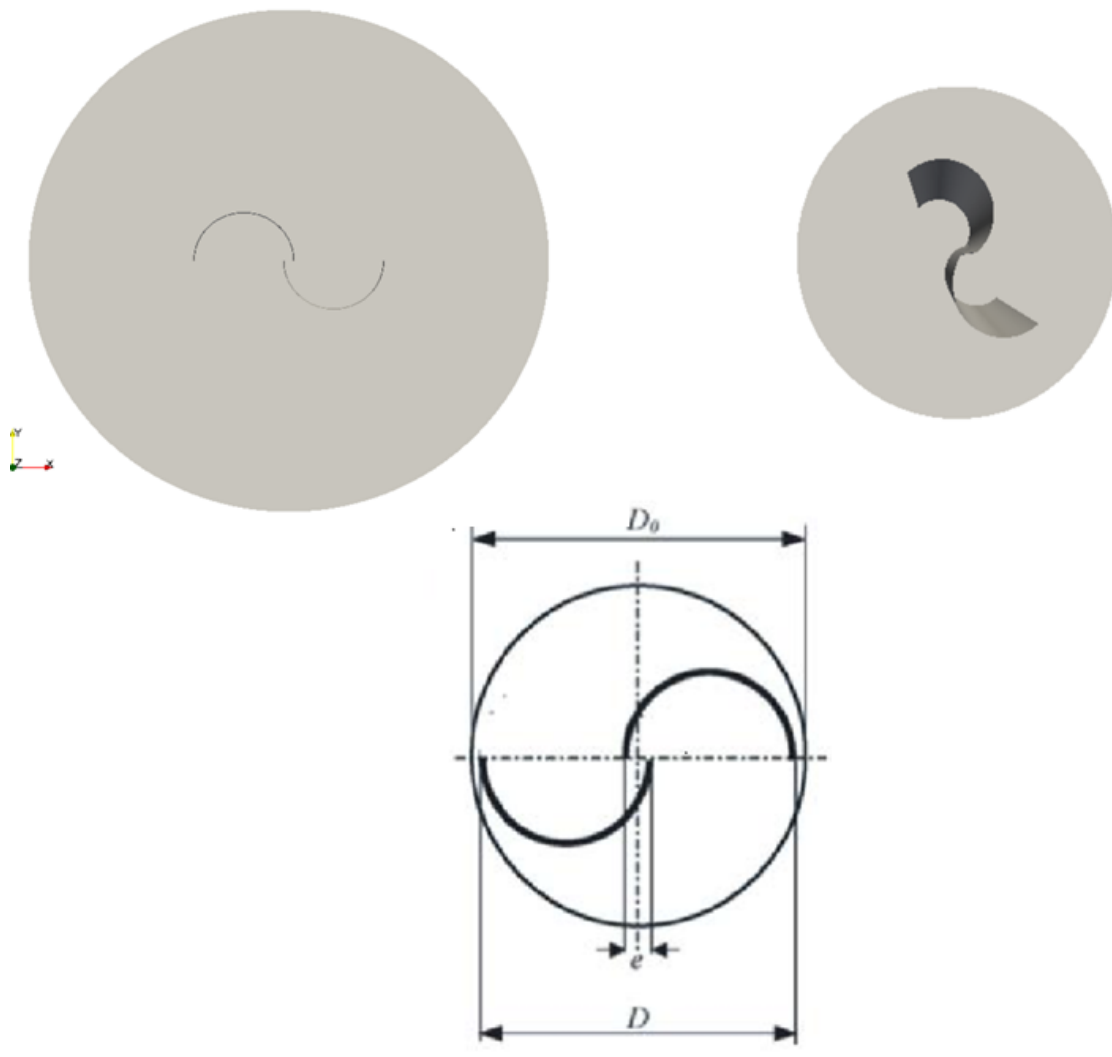
Figure 4.2: Rotor geometry

At the same time, the stator takes on a rectangular shape that is large enough to ensure the visualization of the flow behavior at infinity..

the rectangle contains a circle of the same diameter as the rotor to allow the two geometries to be assembled. The stator dimension is 40D from inlet to outlet and 20D from top and bottom of the calculation area figure 4.3.
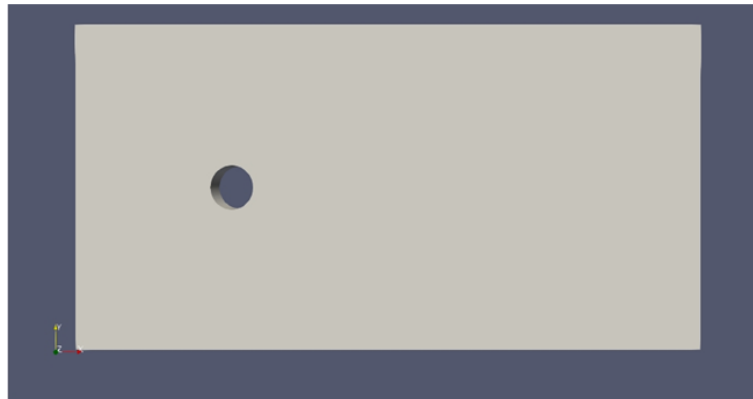
Figure 4.3: Stator geometry

The calculation domain is represented by the figure 4.4:
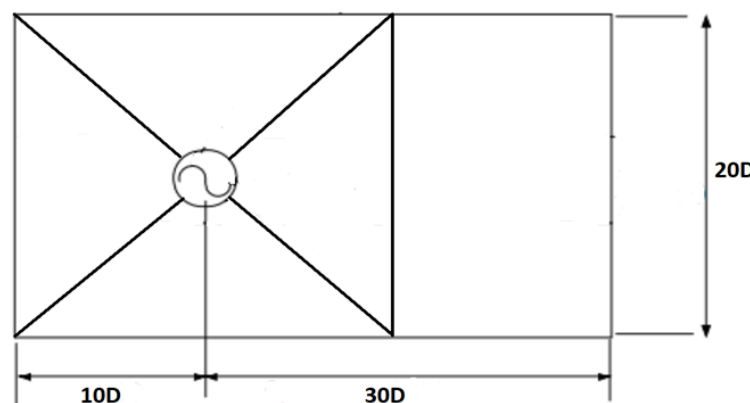
Figure 4.4: Calculation domain

For the mesh we used the hybrid type generated in the two geometries that are presented in the figure 4.5 and the figure 4.6.
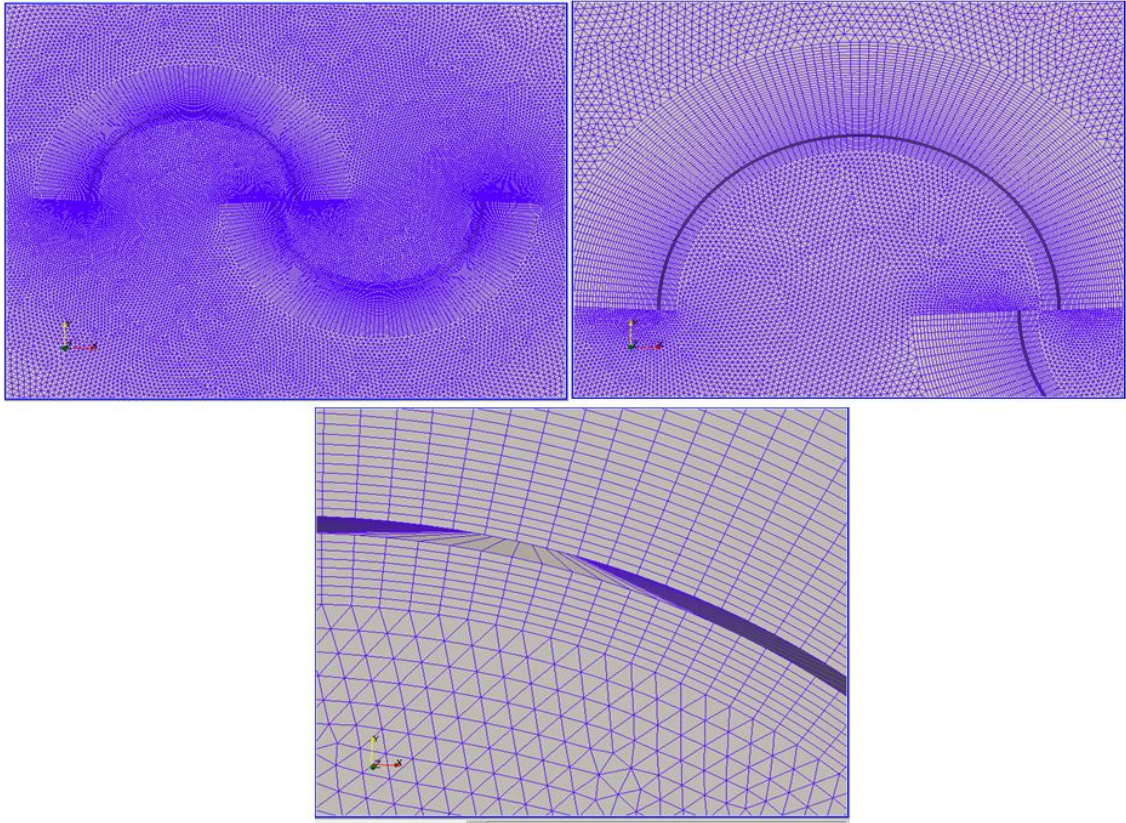
Figure 4.5: Rotor mesh
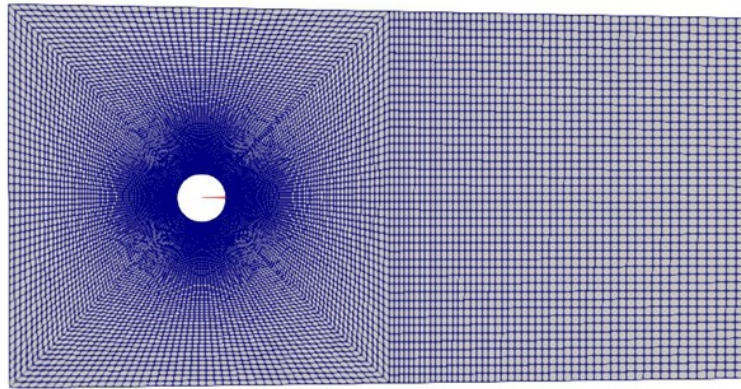
Figure 4.6: Stator mesh

For the boundary layer, the thickness "s" of the first sub-layer must be calculated, knowing that the Reynolds number is given by the following formula :

$$R_e = \frac{\rho U_\infty D}{\mu} \tag{4.27}$$

with:

D: diameter in m

μ: the dynamic viscosity of the air:μ=0.000018375(kg/m.s).

ρ:the density of the air:ρ=1.225(kg/m^3).

U$_\infty$: the upstream flow velocity: U_∞= 10 m/s.

then, by finding : R_e=146000. Knowing the Reynolds number, we can calculate the friction coefficient C_f the wall friction rate$\tau_{wall}$and the friction speedU_{fric}.

$$C_f = \frac{0.026}{R_{ex}^{\frac{1}{7}}} \tag{4.28}$$

$$\tau_{wall} = \frac{C_f \rho U_\infty^2}{2} \tag{4.29}$$

$$U_{fric} = \sqrt{\frac{\tau_{wall}}{\rho}} \tag{4.30}$$

By applying the wall function ,so we can determine the thickness of the 1st boundary layer :

$$s = \frac{y^+ \mu}{U_{fric}\rho} \tag{4.31}$$

4.4.3   The initial conditions

The initial conditions define the starting values of each solution. They therefore play an essential role in the stability and computation time of the simulations. To ensure a good convergence rate of the simulation, it is good to initialize the domain near the expected solution Before starting our simulation, some parameters must be initialized. The turbulence parameters are imposed as shown below :

-Turbulent kinetic energy :

$$k = 1.5 U_\infty^2 I^2 \tag{4.32}$$

where: I is the turbulent intensity.

-The dissipation rate of the turbulent kinetic energy :

$$\epsilon = 10 C_\mu \frac{K^1.5}{K D_h} \tag{4.33}$$

-The specific dissipation rate :

$$\omega = \frac{1}{\epsilon} \tag{4.34}$$

4.4.4 Boundary conditions

Identify the location of boundaries (e.g., inlet, outlet, symmetry) as shown in the figure 4.7.

-Inlet : it is imposed upstream of the calculation domain, as an entry condition of the flow.

-Outlet : it is imposed at the downstream end of the calculation domain, as an exit condition of the flow.

-Symmetry : The symmetry plane boundary condition is used to apply mirror symmetry conditions on a structure, If a symmetry plane condition is applied to a face, the displacement of that face is locked in the normal direction but free to slide in the tangential directions.

-Interface cyclic AMI : it is a common condition between the circular surface of the fixed part (stator) and that of the mobile part (rotor), it allows to transfer the data of the cells of these two parts.
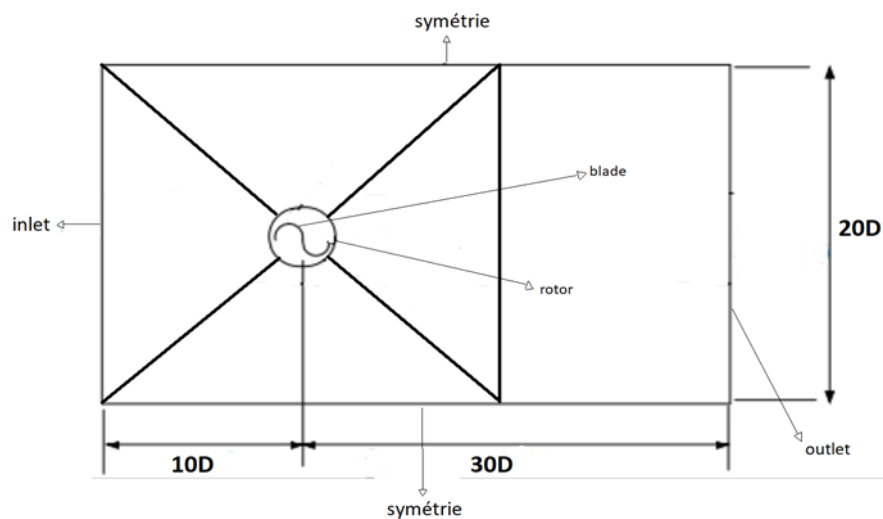
Figure 4.7: Boundary conditions

4.4.5 OpenFoam

Is a free and open source CFD toolkit. OpenFOAM stands for "Open source Field Operation and Manipulation". It is used in universities and industry to solve a wide variety of computational problems. Unlike any proprietary software, the source code here is accessible and modifiable.OpenFOAM has enormous capabilities. There is a huge database of solvers that covers the breadth and depth of CFD.

OpenFOAM solvers include :

- Incompressible flow with RANS and LES capacities.

- Compressible flow solvers with RANS and LES capabilities.

- solid dynamics.

- combustion problems.

- combined heat transfer.

- molecular dynamics.

- electromagnetism.

OpenFOAM utilities are divided into several categories :

Mesh conversion   Utilities to convert to OpenFOAM format the mesh generated by third party meshing tools like Ansys, Gambit.

Parallel processing   Tools to decompose, reconstruct and redistribute the calculation case to perform parallel calculations, sometimes better than other CFD software.

Post-processing   Data can be visualized using paraview, they can be exported to other software to be visualized.

PimpleFoam   Transient solver for incompressible and turbulent Newtonian fluid flow, with optional mesh motion and modification of the mesh topology.

SimpleFoam   Steady state solver for incompressible and turbulent flows, using the SIMPLE (Semi-Implicit Method for Pressure Linked Equations) algorithm.

4.4.6   Simulation by OpenFoam

When the meshes are finished in Gambit, the next step is to import the meshes into the openfoam solver and assemble the 2 geometries (stator and rotor) and to do this you need to know some essential codes to use in OpenFoam like:

- run: to launch OpenFoam.

- cd : the name of the folder or file you want to open.

- ls : to view the folder names .

- code GambitToFoam : to convert the Gambit format to OpenFoam format.

- mergemeshes : To assemble the two meshes (stator and rotor) in a single polymesh file.

-paraFoam : To launch the processor station paraview.

in our case we have imported the geometry of the stator and rotor and we have assembled the two meshes we have obtained a mesh (polymech) which is presented in the figure 4.8.

Figure 4.8: Stator and rotor assembly

Before starting the simulation, it is necessary to check and modify the three files (system, constant, 0) figure 4.9.

Constant file This file contains all the constants of the problem: there are the physical properties, (transport Properties and turbulence models). It also contains a sub-file poly-Mesh which presents all the information about the mesh.

System folder In this file you can change the parameters concerning the resolution of the problem. It contains at least the files following: (controlDict) where we find the parameters like time step, final time.. (fvSchemes) where we can select the discrestization schemes, and (fvSolution) where we can choose the parameters and the solver for the execution, (decomposeParDict) allows the calculation in parallel in order to minimize the calculation time.

File 0 This file contains all the information concerning the parameters we want to visualize (speed, pressure for example) to define the problem, and also it contains the results written by OpenFOAM.
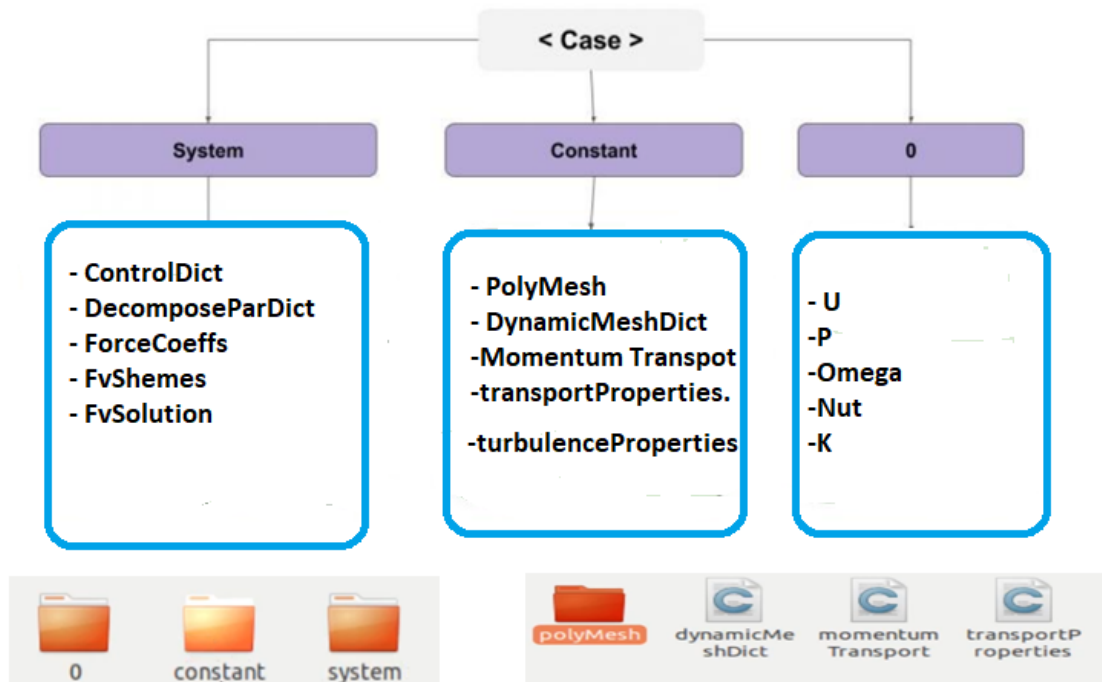
Figure 4.9: Information files and simulation parameters

The calculation can be started using the following command :

pimpleFoam which calls the algorithm needed to solve the problem.

At the end the results are displayed in the postProcessing folder and we use qtiplot to view the results of the simulation.

Chapter 5

Results and Discussion

5.1 Introduction

In this chapter, the results of the numerical simulation will be presented and interpreted using the solution of the Navier-Stockes equations for an incompressible 2D flow. The mesh independence that allows to obtain accurate results is studied, then the influence of lambda on the wake is presented, and the results are compared with experimental values obtained by Fawaz and Dobrev [26].

5.2 Mesh independence

In this part, we start by choosing the most appropriate mesh comparing to the experimental values[26]. For each mesh a simulation of an incompressible flow is performed at U_∞=10 m/s around a Savonius rotor, different values (mechanical torque, rotor power, power coefficients) are obtained and the closest value to the experimental one is chosen, these results are presented in the following table (table 5.1):

	mesh1	mesh2	mesh3	mesh4	exp
Q	0.77	0.69	0.68	0.48	0.43
P	41.99	37.63	37.08	26.12	23.45
C_p	0.31	0.273	0.275	0.19	0.17
ΔC_p	0.14	0.103	0.105	0.02	

Table 5.1: *Mesh independence*

with:

$$\Delta C_p = |C_p(exp) - C_p(mesh)|$$

We notice that the value of the power coefficient of mesh 4 is closer to the experimental value, so we chose mesh 4 to examine the other results. The parameters of this mesh are the following :

-number of elements:

stator : 16650 elements.

rotor : 63694 elements.

- We chose 's' after several simulations, the best case was s=0.0005 for $U_\infty = 10 m/s$ and $U_{local} \approx 28 m/s$ and for $y^+ \approx 55$.

5.3   Study of mechanical torque

According to the OpenFoam simulation we obtained the parameter of the mechanical torque from the calculation of the parameters of the moment (pressure, viscosity) in relation to the Z axis (axis of rotation) so it is the average of the summation of the column 13 and 16 which is represented in the file force.dat in the folder postprocessing which is shown in the figure 5.1:

knowing that the first column corresponds to the physical time, the 9 following columns

Figure 5.1: The results of Moment

correspond to the Force (3 columns for the Pressure force + 3 columns for the viscous force

+ 3 columns for the porosity), the columns from 11 to 19 correspond to the moment.

using Qtiplot, we plot the sum of the two columns and obtain the moment versus time curve as in the figure 5.2, and the red line represents the average moment which physically means the mechanical torque.
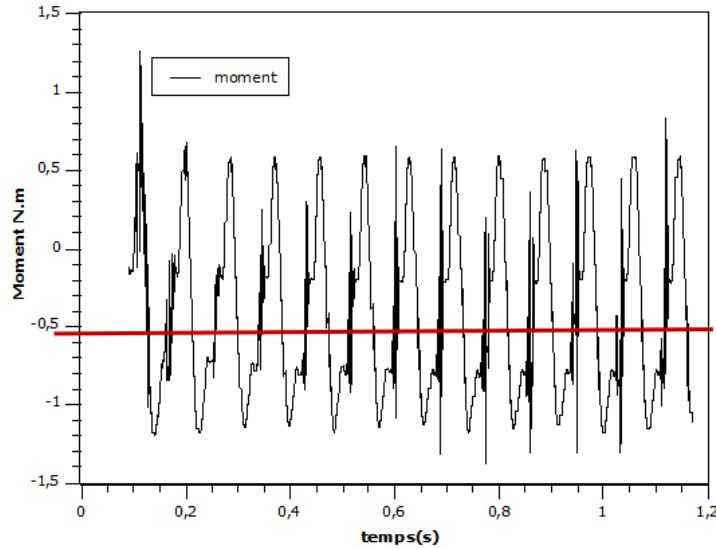
Figure 5.2: Variation of Moment as a function of Time

5.4 Validation of results

for the validation of the results we take the experimental (obtained by the PIV method) and numerical researches of Fawaz Massoouh and Dobrev [26] as a reference and compared them with our numerical results obtained with Openfoam.The power coefficient C_p for different λ(0.6, 0.8 and 1.05),is illustrated in the following table (table 5.2).

with :

-Error1=$|C_p$ experimental -C_p simulation OpenFoam present work |.

-Error2=$|C_p$ experimental -C_p simulation,2D,$K\omega - SST$ reference [26] |.

-Error3=$|C_p$ experimental -C_p simulation,3D,$K\omega - SST$ reference [26] |.

-Error4=$|C_p$ experimental -C_p simulation,3D,DES/$K\omega - SST$ reference [26] |.

In this case we obtained our simulation results of power coefficient closer to the experimental results because the error1 is smaller than the other error like it is illustrated in the table (5.2), which justifies the effectiveness of the model that we used in this work.

Power coefficient C_p	λ=0.6	λ=0.8	λ=1.05
C_p experimental	0.176	0.180	0.167
C_p simulation OpenFoam present work ,2D,$K\omega - SST$	0.19	0.200	0.17
Error1	0.014	0.02	0.003
C_p simulation,2D,$K\omega - SST$ reference [26]	0.182	0.208	0.207
Error2	0.006	0.028	0.04
C_p simulation,3D,$K\omega - SST$ reference [26]	0.141	0.147	0.139
Error3	0.035	0.033	0.028
C_p simulation,3D,DES/$K\omega - SST$ reference [26]	0.172	0.176	0.149
Error4	0.004	0.004	0.018

Table 5.2: *Experimental and numerical results*
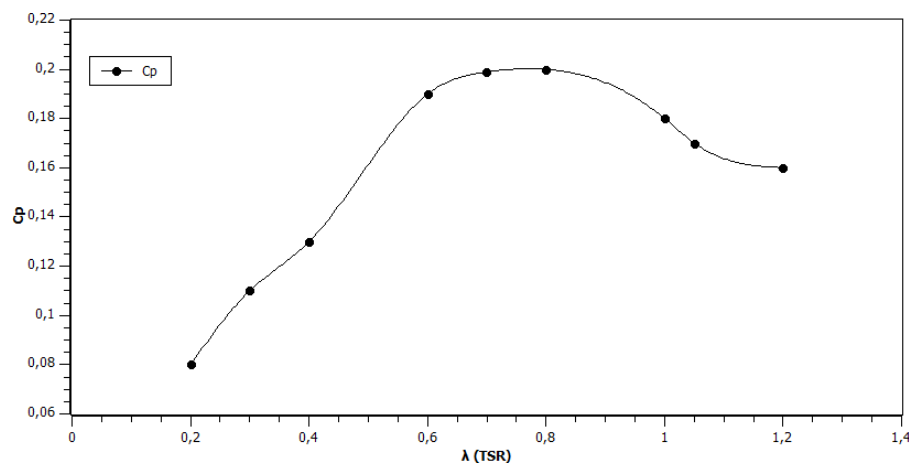
Figure 5.3: variation of C_p as a function of λ

The curve shows the variation of the power coefficient according to different values of lambda (see figure 5.3) the curve justifies the Betz limit which says that a wind turbine has a maximum C_p for a specific rotation speed, so we notice in the curve that the C_p increases until reaching the maximum C_p for the specific rotation speed and then decreases when the rotation speed increases from the specific value.

5.5   Variation of aerodynamic coefficients

Firstly the aerodynamic coefficients are plotted using Qtiplot, the coefficients of moment, lift and drag are shown in the figures below ,we noticed that there is a variation of frequency for each value of λ which means that the increase of the rotation speed influence of frequency and wave length, which means that there is a proportionality relation.
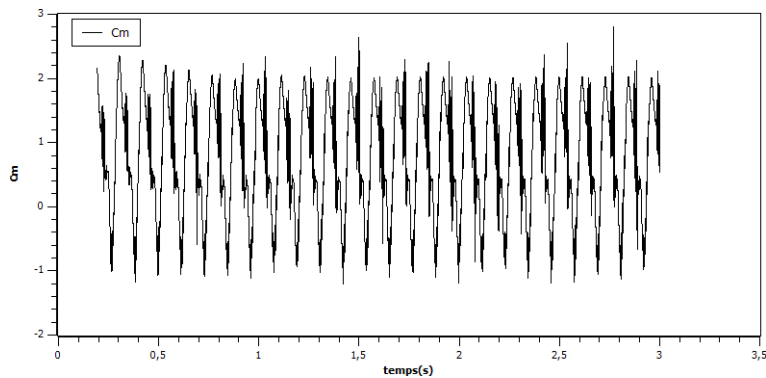
Figure 5.4: C_m coefficients for λ= 0.6
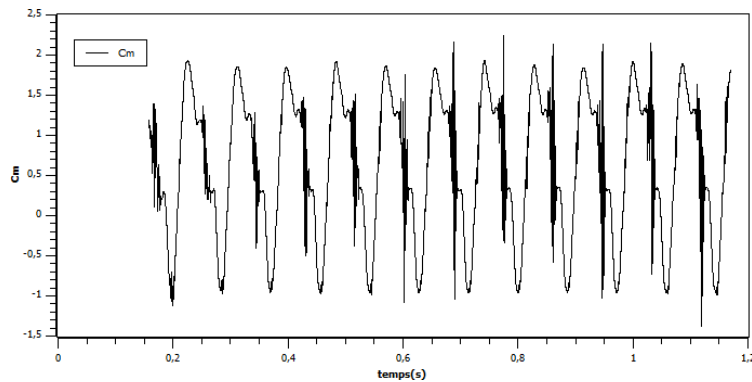
Figure 5.5: C_m coefficients for λ= 0.8
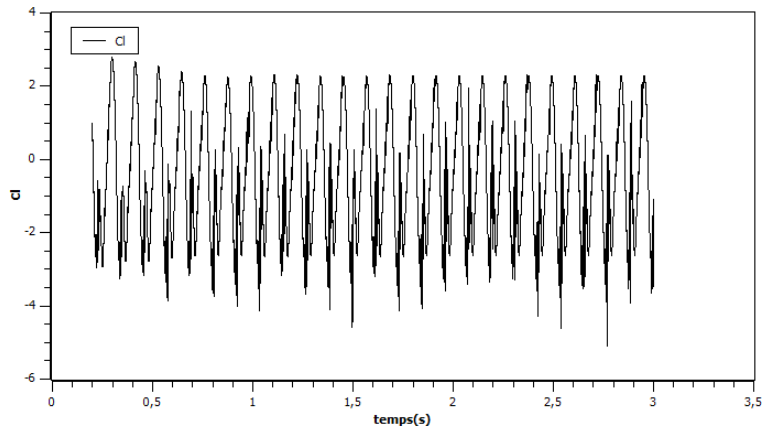
Figure 5.6: C_l coefficients for λ= 0.6
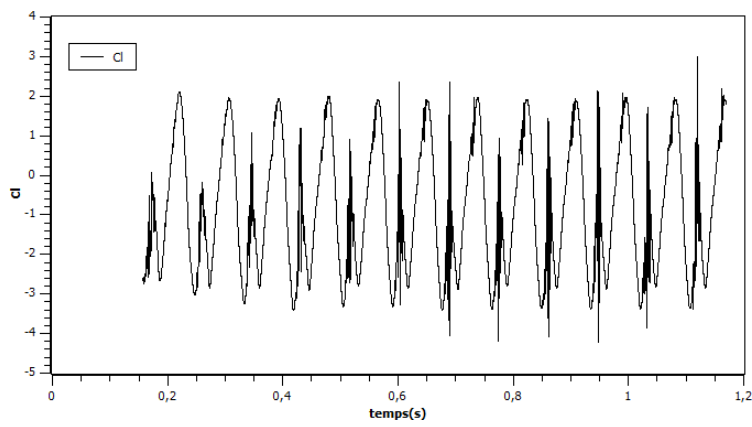
Figure 5.7: C_l coefficients for λ= 0.8
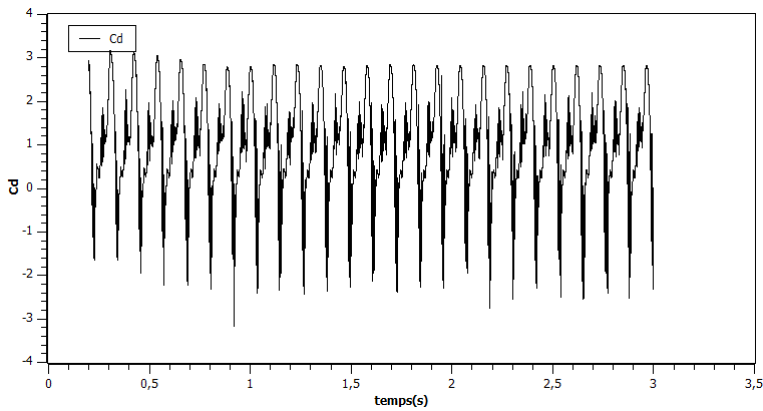
Figure 5.8: C_d coefficients for λ= 0.6
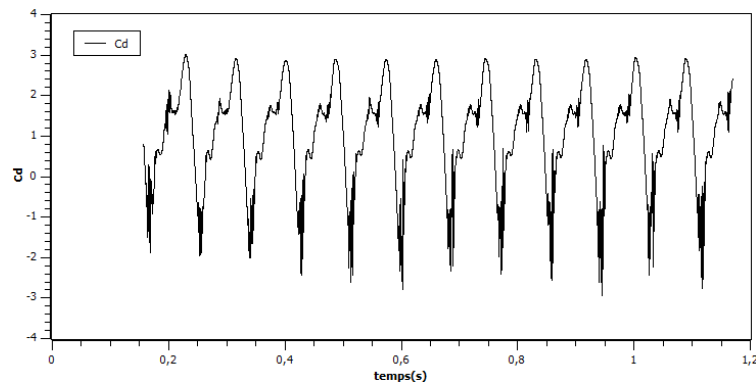
Figure 5.9: C_d coefficients for $\lambda = 0.8$

5.6   Velocity contours around the Savonius

On the figures below , we note 3 particular zones The intrados of the blade one, is a depression zone, which constitutes a certain resistance which tends to slow down the blade.

the intrados of the blade two , this zone attends an overpressure which tends to make the blade turn in the positive direction.Zone corresponding to the blade tips. These two zones are subject to the influence of a turbulence due to the edge effect and to the acceleration of the particles generated by the curvature of the blades The contours of the velocity and

the streamlines are shown in (5.10),(5.11),(5.12),We can see that at the first instant, the current lines are narrowing while getting closer to the resisting blade, while the phenomenon is less nuanced on the side of the driving blade. This narrowing is more nuanced at the end of the blade and the current lines tend to turn back towards the lower surface of the same blade. Figures 5.10,5.11,5.12, shows the distribution of the velocity around our wind turbine which is facing a flow of 10m/s for different values of λ and different angles(0°,30°,60°,90°,120°,150°), We notice that the intensity of the wake increases with the increase of λ ,in addition the ve- locity in the blade tip increase due to the effect of the rotor rotation and sweeping the air in the rotation direction.

5.7 Vorticity

This is the rotational velocity field, expressed as :

$$\Psi = rotV$$

first of all, concerning the interactions between scales of motion, it is non-linear term that will allow the kinetic energy to be transported from movements of a certain size to movements of another size. This flow of energy will be towards the small scales allowing the phenomenon of viscous dissipation of the kinetic energy.

The figures(5.13)(5.14)and(5.15) below present distribution of vorticity with different λ for different angles (0°,30°,60°,90°,120°,150°),we notice that the intensity of the Vortex increases with the increase of λ.

The contours of the vorticity constitute vortex zones of the fluid, these vortices diffuse and take up more and more space while disappearing far into the flow.

(a) *Angle, θ = 0*

(b) *Angle, θ = 30*

(c) *Angle, θ = 60*

(d) *Angle, θ = 90*

(e) *Angle, θ = 120*
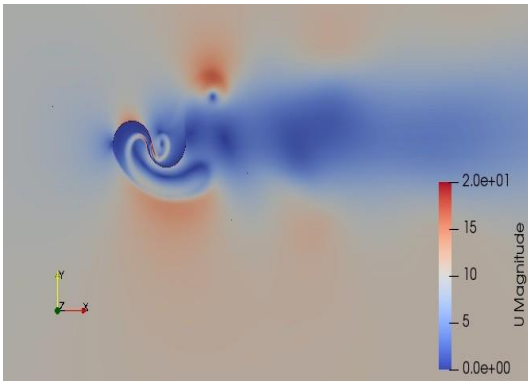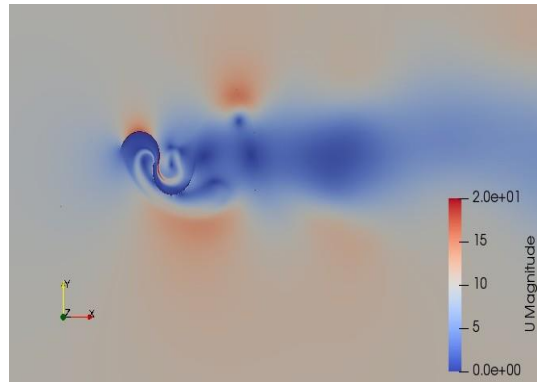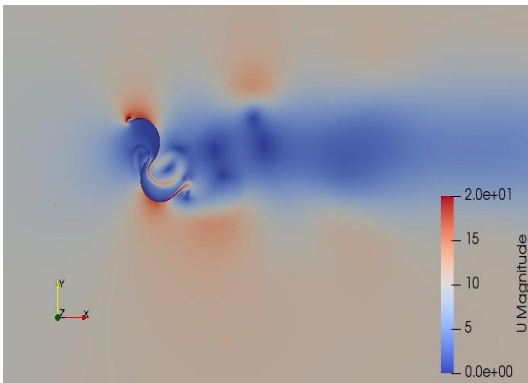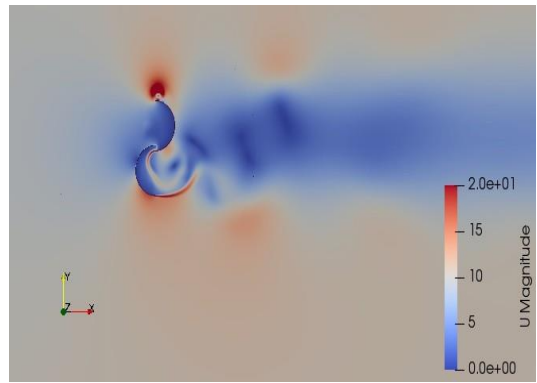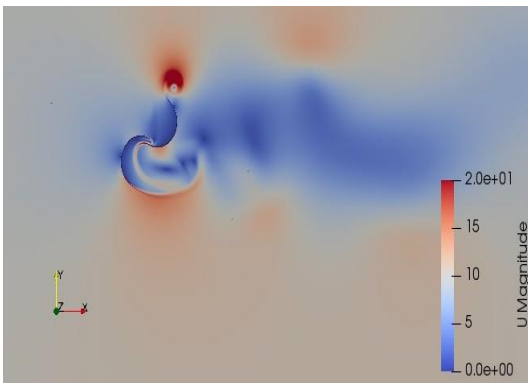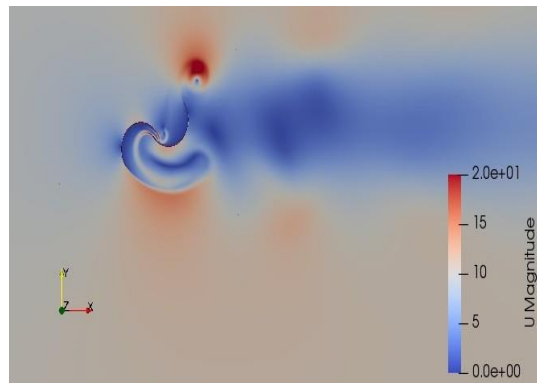
(f) *Angle, θ = 150*

Figure 5.10: Velocity distribution with $\lambda = 0.6$ around Savonius for different angles.

(a) *Angle, θ = 0*

(b) *Angle, θ = 30*
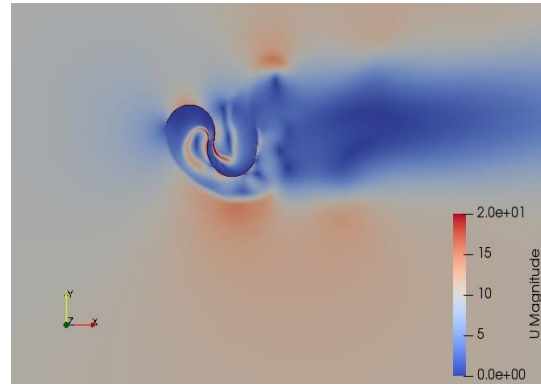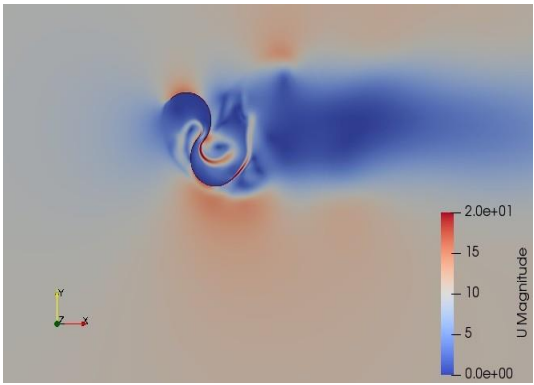
(c) *Angle, θ = 60*

(d) *Angle, θ = 90*

(e) *Angle, θ = 120*
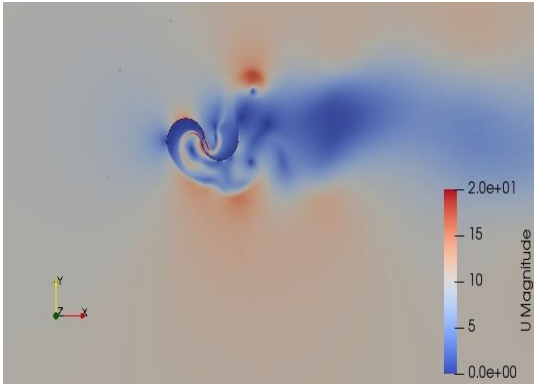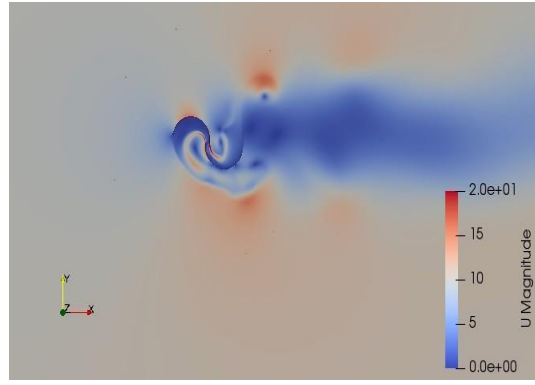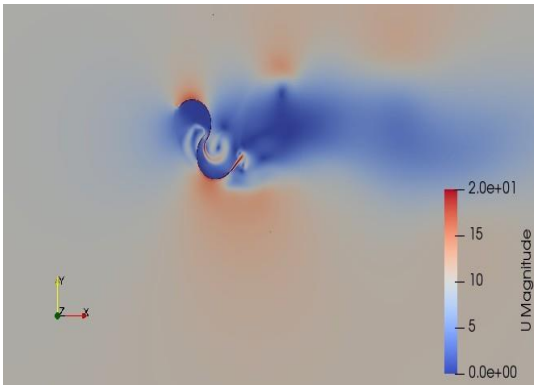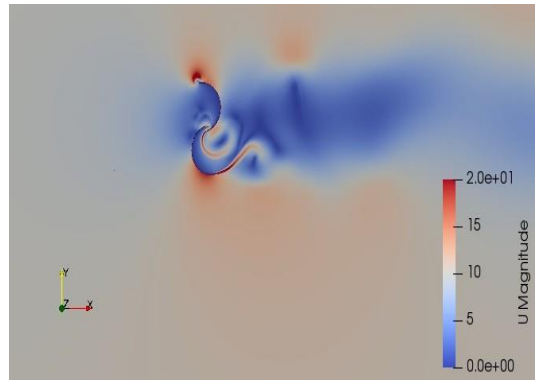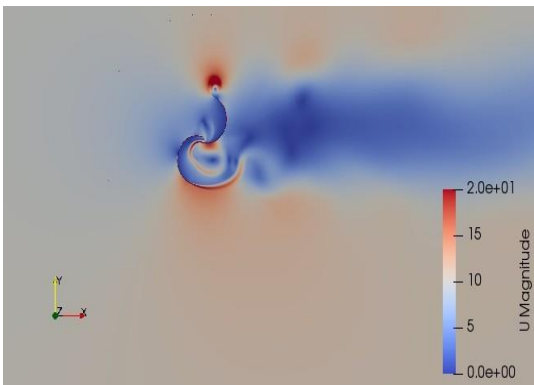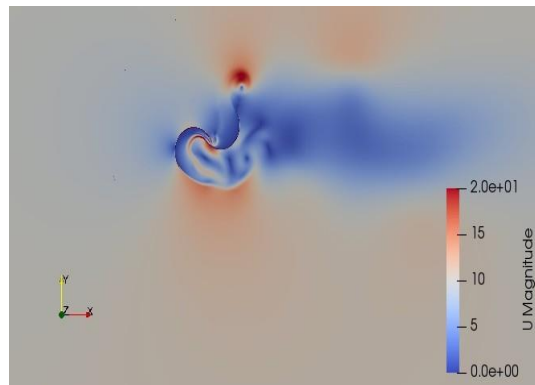
(f) *Angle, θ = 150*

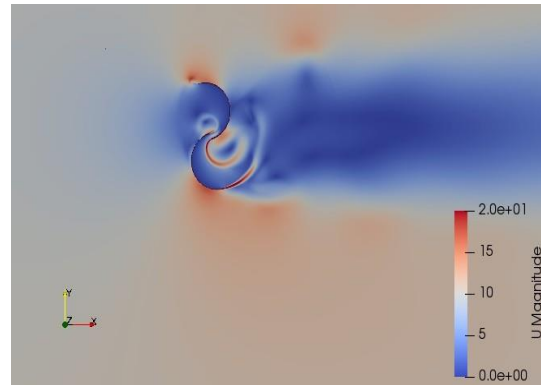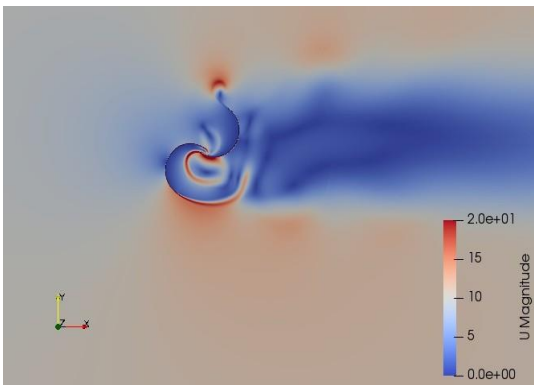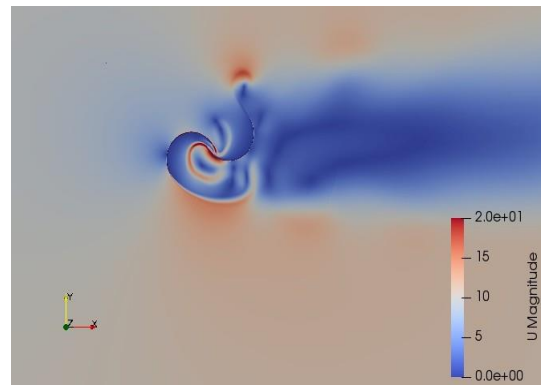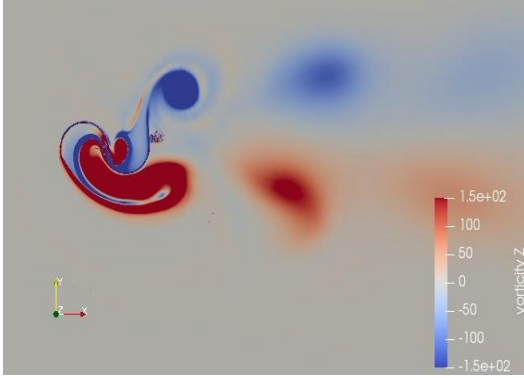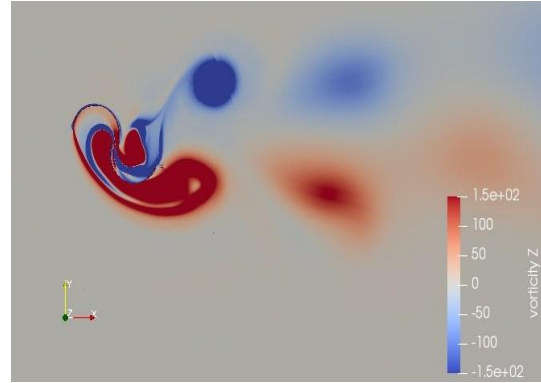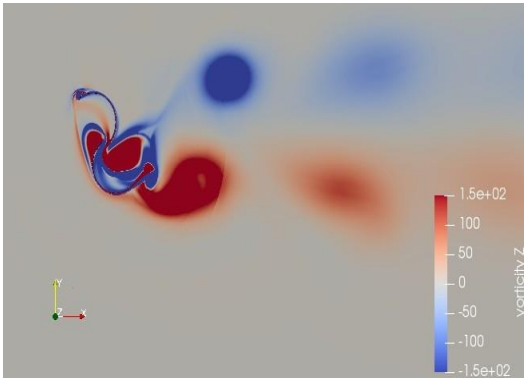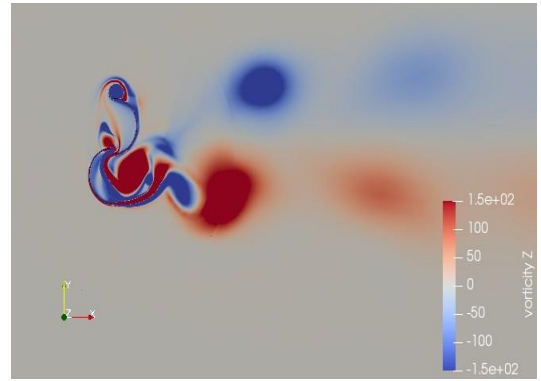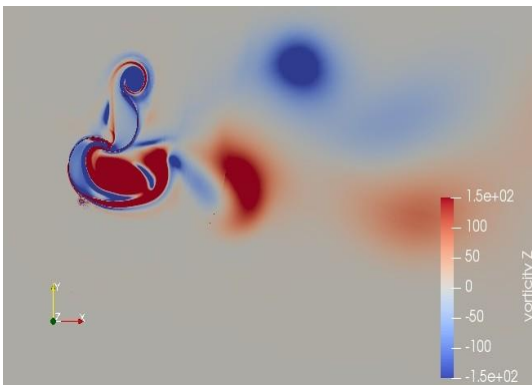Figure 5.11: Velocity distribution with $\lambda = 0.8$ around Savonius for different angles
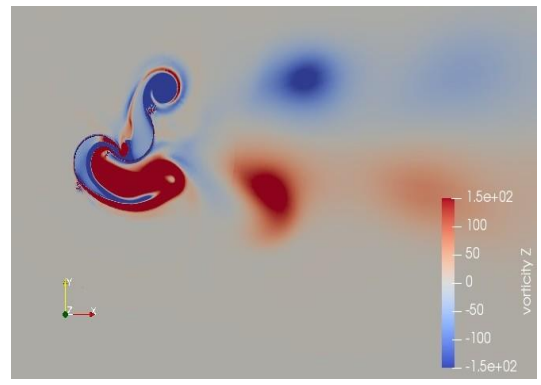
(a) *Angle, θ* = 0

(b) *Angle, θ* = 30

(c) *Angle, θ* = 60

(d) *Angle, θ* = 90

(e) *Angle, θ* = 120
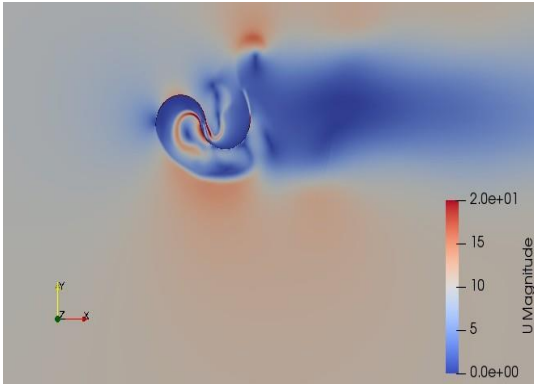
(f) *Angle, θ* = 150

Figure 5.12: Velocity distribution with λ = 1.05 around Savonius for different angles

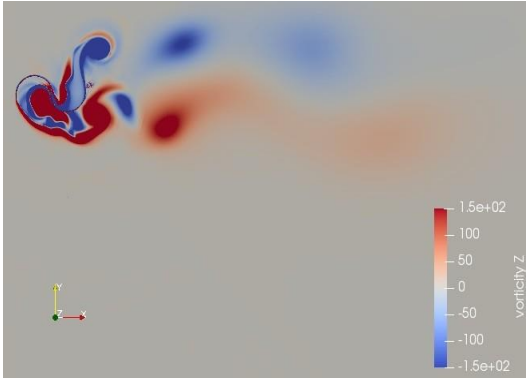(a) *Angle, θ* = 0

(b) *Angle, θ* = 30

(c) *Angle, θ* = 60

(d) *Angle, θ* = 90

(e) *Angle, θ* = 120

(f) *Angle, θ* = 150

Figure 5.13: Vorticity with λ = 0.6 around Savonius for different angles

(a) *Angle, θ* = 0

(b) *Angle, θ* = 30

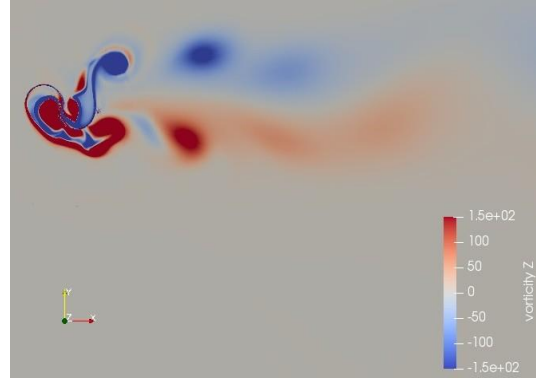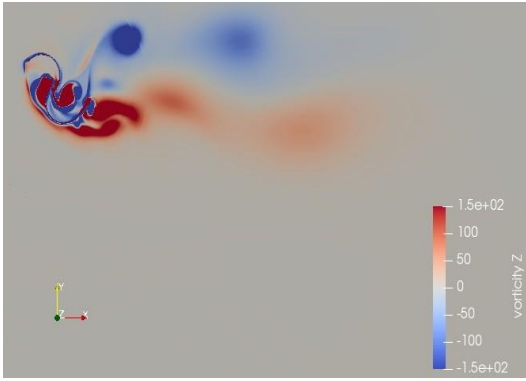(c) *Angle, θ* = 60

(d) *Angle, θ* = 90

(e) *Angle, θ* = 120
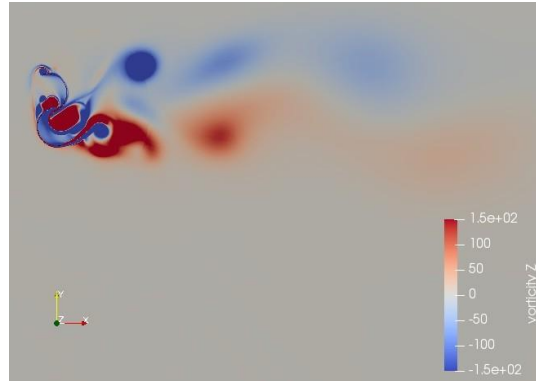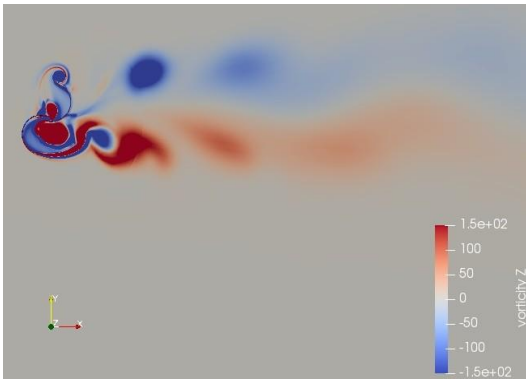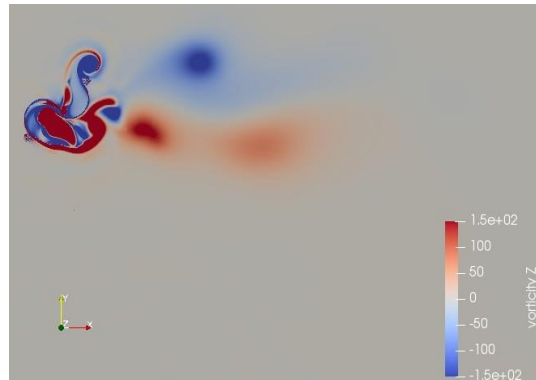
(f) *Angle, θ* = 150

Figure 5.14: Vorticity with λ = 0.8 around Savonius for different angles

(a) *Angle, θ* = 0

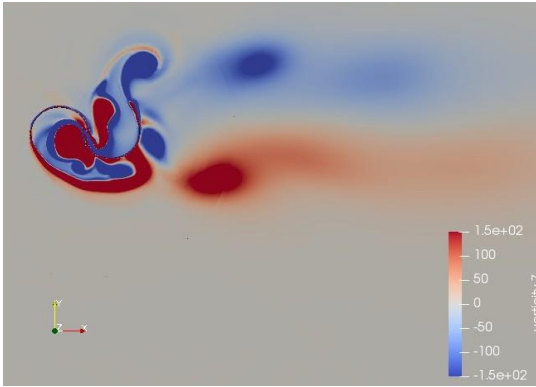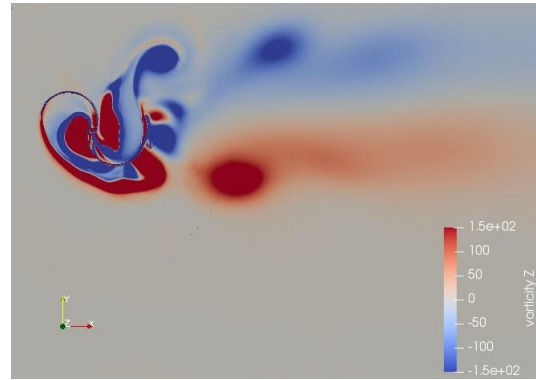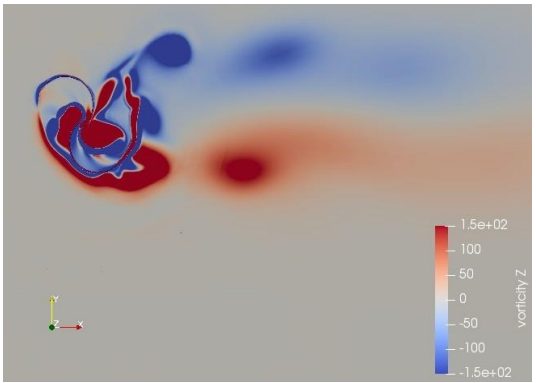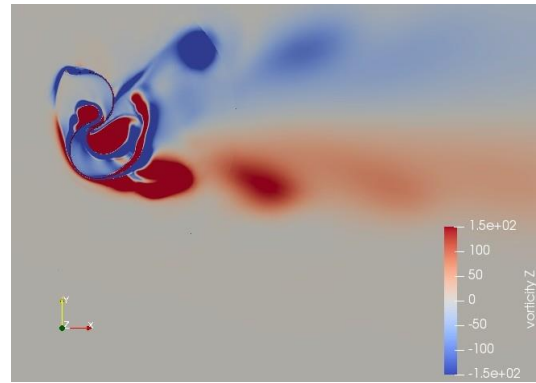(b) *Angle, θ* = 30

(c) *Angle, θ* = 60

(d) *Angle, θ* = 90

(e) *Angle, θ* = 120
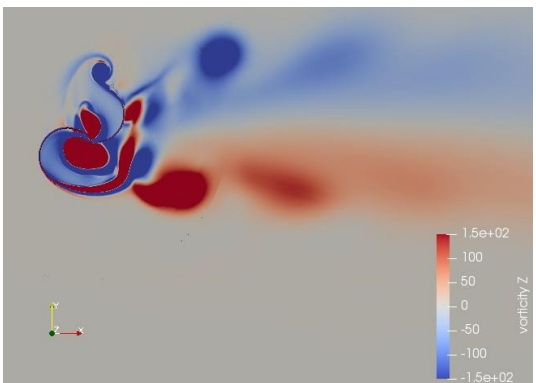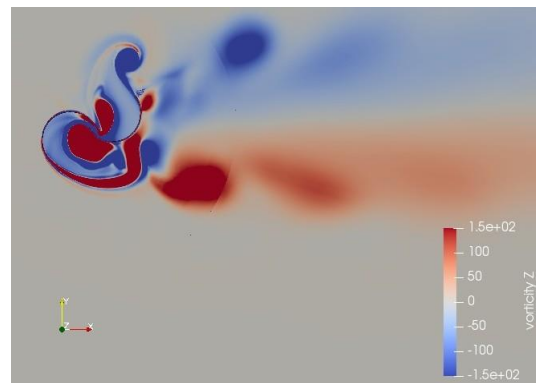
(f) *Angle, θ* = 150

Figure 5.15: Vorticity with λ = 1.05 around Savonius for different angles

CONCLUSION

With the problems of pollution and the exhausting of fossil energy sources, the the world is now interested in the development of clean and renewable energies, which justifies the diversity of scientific research obtain in this field.

In our study we have focused on the analysis of Numerical modeling of turbulent flow and the wake generated around a vertical axis wind turbine of the SAVONIUS type with the CFD code OpenFoam which is based on the finite volume method for solving the RANS equations. Based on studying the mesh independence we focus to realize the appropriate mesh for our simulation to obtain better result , thereafter by choosing the best mesh that we obtain from the study we continue the simulation with OpenFoam using the K ω-SST turbulence model to get the results of different aerodynamics coefficients (Moment ,lift ,drag), also the coefficient of power, contours of velocity and vorticity around Savonius wind turbine .

We compared the variations of the power coefficient with the specific velocity λ or (TSR). The results obtained are in good agreement with the experimental work available in the reference that justify also the proper choice of K ω-SST . After validation of our calculation we present the aerodynamics coefficients (Moment ,lift ,drag) as function of time in form of graphs with different values of λ, in addition the contours of velocity and vorticity with several values of λ around Savonius wind turbine for different angles showing that the wake intensity its increases by increasing λ .

Finally, Savonius wind turbine is a self-starting vertical axis rotor. It can be designed to be compact in size and also produces less noise which makes it suitable to integrate into urban spaces . These characteristics make it interesting from a sustainability point of view, especially when aiming to increase the decentralization of electricity production.

REFERENCES

1. William A. EDELSTEIN et Ge R&D : A report prepared for the panel on public affairs (popa), american physical society. *WIND ENERGY,*2003.

2. Ammar Sami PARASCHIVOIU, Ion et Farooq SAEED : a comparative performance study of 2 6 mw rated capacity turbines. *Transactions of the Canadian Society for Mechanical Engineering*, 42(4):393–403, 2018.

3. *IEA, Key Word Energy Statistics, 2002*.

4. *GWEC, Global Wind Energy Council 2006, Global Wind Energy Outlook 2006*.

5. A. H. BENESH : Wind turbine with savonius-type rotor, 1996.

6. E. HAU : *Wind turbines: fundamentals, technologies, application, economics*. Springer Science Business Media, 2006.

7. *http://awea.org/learnabout*.

8. *http://www.windpower.org/en/*.

9. *http://www.eia.gov/cneaf/solar.renewables/page/wind/wind.html*.

10. AD. HANSEN, P. SORENSEN et F. BLAABJERG : Centralised power control of wind farm with doubly fed induction generators. *Renewable and sustenabel energy*, 31:935–951, 2006.

11. *http://www.parc-eolien-mont-des-quatre-faux.f / lenergie-eolienne/ comment-ca-marche*.

12. S. El AIMANI : *Modélisation des différentes technologies d éoliennes intégrées dans un réseau de moyenne tension*. Thèse de doctorat, Université des sciences et tech-nologies de Lille, 2004.

13. P. Sen S. Kouro M. Nariman V. YARAMASU, B. Wu : Computer science proceedings. *IEEE*, 2015.

14. M. A. LARABI : Conception de la commande d une machine asynchrone destinée á l énergie renouvelable, Université des Sciences et de la Technolo- gie d Oran Mohamed Boudiaf, 2018.

15. D. CHENITI & K. ALILICHE : *Etude analytique et numérique du coeeficient de puissance d une eolienne savonius a axe vertical a 2 et 3 pales.* Thèse de doctorat, Université de M sila, 2020.

16. *https://jardi-brico.com/les-differents-types-deoliennes/.*

17. *https://www.ecosources.info/dossiers/EolienneverticaleSavonius.*

18. S.J. SAVONIUS : The s-turbine and its application. *Mechanical Eng*, 53(5):333–338, 1931.

19. L. CHANG : Systémes de conversion de l'energie eolienne. *IEEE Canadian*, pages 1–5, 2002.

20. B. MULTON : Aérogénérateurs electriques. *Editions GEEA, Cachan*, 2004.

21. Z. HAMMI MEDJDOUB & A. OULD MOHAMED YAHYA : Intégration et stratégie de contrôle de la production éolienne au réseau électrique Ã base de la machine synchrone á aiment permanent. Mémoire de D.E.A., Faculté des Sciences et de la Technologie, 2016.

22. Bhattacharya S. Jain A. & Paul A. R DESHMUKH, S. : Wind turbine noise and its mitigation techniques. *Energy Procedia*, 160:633–640, 2019.

23. *https://www.les-energiesrenouvelables.eu/conseils/eolienne/realiser-projet-eolienne/bruit-eoliennes/.*

24. S. M. BOUDIA : *Optimisation de l évaluation temporelle du gisement énergétique éolien par simulation numérique et contribution á la réactualisation de l atlas des vents en Algérie.* Thèse de doctorat, Université de Tlemcen, 2013.

25. *https://www.energysage.com/about-clean-energy/wind/pros-conswind-energy/.*

26. I.Dobrev et F.MASSOUH : Cfd and piv investigation of unsteady flow through savonius wind turbine. *Energy Procedia*, 6:711–720, 2011.

27. H.Sutanto F.Wᴇɴᴇʜᴇɴᴜʙᴜɴᴀ, A. Saputraa : An experimental study on the performance of savonius wind turbines related with the number of blades. *Energy Procedia*, 68:297–304, 2015.

28. EL-HAROUN A. A. WAHBA MAHMOUD, N. H. : An experimental study on improvement of savonius rotor performance. *Alexandria Engineering*, 51(1):19–25, 2012.

29. Song Baowei-Vanzwieten James h. Tɪᴀɴ, Wenlong : Computational fluid dynamics prediction of a modified savonius wind turbine with novel blade shapes. *Energies*, 8(8):7915–7929, 2015.

30. Mohamed Salah Dʀɪss, Zied et Abid : Numerical investigation of the aerodynamic structure flow around savonius wind rotor. *Science*, 2(2), 2012.

31. Biswas A. Sharma K Gʜᴏsʜ, A. : Computational analysis of flow physics of a combined three bladed darrieus savonius wind rotor. *Energy Institute*, 88(4):425–437, 2015.

32. Liskiewicz Grzegorz et Sobczak Krzysztof Kᴀᴄᴘʀᴢᴀᴋ, Konrad : Numerical investigation of conventional and modified savonius wind turbines. *Renewable energy*, 60:578–585, 2013.

33. Jessen Marius Stette Bracchi Tania Aʟɪꜰᴇʀɪs, Alexander D. : Performance and wake of a savonius vertical axis wind turbine under different incoming conditions. *Wind Energy*, 22(9):1260–1273, 2019.

34. Aggour M. et Toumi Zᴇᴍᴀᴍᴏᴜ, M. : Review of savonius wind turbine design and performance. *Energy Procedia*, 141:383–388, 2017.

35. Abd El-Hamid A. A. El-Askary Gᴀᴅ, H. E. : new design of savonius wind turbine: numerical study. *CFD letters*, 6(4):144–158, 2014.

36. Chan Chun Man Zhu X. Bᴀɪ, H. I. : A numerical study on the performance of a savonius-type vertical-axis wind turbine in a confined long channel. *Renewable Energy*, 139:102–109, 2019.

37. Montelpare S. Ricci R. D.Aʟᴇssᴀɴᴅʀᴏ, V. : Unsteady aerodynamics of a savonius wind rotor: a new computational approach for the simulation of energy performance. *Energy*, 35(8):3349–3363, 2010.

38. Mohammed Hadi ALI : Experimental comparison study for savonius wind turbine of two & three blades at low wind speed. *International Journal of Modern Engineering Research (IJMER)*, 3(5):2978–2986, 2013.

39. Nachida. MENET, Jean-Luc et Bourabaa : Increase in the savonius rotors efficiency via a parametric investigation. *European Wind Energy conference & exhibition*, pages 22–25, 2004.

40. Adam M RAGHEB, Magdi et Ragheb : Wind turbines theory-the betz equation and optimal rotor tip speed ratio. *Fundamental and advanced topics in wind power*, 1(1): 19–38, 2011.

41. *https://energieplusLesite.be/theories/eolien8/rendement-des-eoliennes/.*

42. Dobrev Ivan et Massouh Fawaz MAALOUF, Bassem : Exploration des structures tourbillonnaires dans le sillage d´un rotor éolien. *1ére Conférence Franco Syrienne sur les énergies renouvelables*, 2010.

43. Christophe Bassem MAALOUF : *Etude des phénomenes tourbillonnaires dans le sillage éolien*. Thèse de doctorat, Arts et Métiers ParisTech., 2010.

44. Kiatkong WORASINCHAI, Supakit et Suwannakij : Performance characteristics of the savonius turbine. *IOP Conference Series: Materials Science and Engineering. IOP Publishing*, 2018.

45. H. A. Vielmo V. AKWA et A. P. PETRY : Review on the performance of savonius wind turbines. *ScienceDirect, Renewable and sustainable energy reviews*, pages 3054–3064, 2012.

46. Dey MANEL : Modélisation numérique du sillage généré par une éolienne á axe vertical de type darrieus tripale. Mémoire de D.E.A., Université SAAD DAHLEB DE BLIDA, 2020.